Atmos. Chem. Phys., 24, 13889–13912, 2024
https://doi.org/10.5194/acp-24-13889-2024

Atmospheric Chemistry and Physics
Open Access
EGU

Research article

The improved Trajectory-mapped Ozonesonde dataset for the Stratosphere and Troposphere (TOST): update, validation and applications

Zhou Zang[1], Jane Liu[1], David Tarasick[2], Omid Moeini[2], Jianchun Bian[3], Jinqiang Zhang[3], Anne M. Thompson[4,5], Roeland Van Malderen[6], Herman G. J. Smit[7], Ryan M. Stauffer[4], Bryan J. Johnson[8], and Debra E. Kollonige[4,9]

[1]Department of Geography and Planning, University of Toronto, Toronto, Canada
[2]Air Quality Research Division, Environment and Climate Change Canada, Toronto, Canada
[3]Key Laboratory of Middle Atmosphere and Global Environment Observation, Institute of Atmospheric Physics, Chinese Academy of Sciences, Beijing, China
[4]Atmospheric Chemistry and Dynamics Laboratory, NASA Goddard Space Flight Center, Greenbelt, MD, USA
[5]GESTAR and Joint Center for Earth Systems Technology, University of Maryland Baltimore County, Baltimore, MD, USA
[6]Scientific Division Observations, Royal Meteorological Institute of Belgium, Brussels, Belgium
[7]Institute for Energy and Climate Research: Troposphere (IEK-8), Research Centre Jülich (FZJ), Jülich, Germany
[8]Global Monitoring Laboratory, NOAA/ESRL Global Monitoring Division, Boulder, CO, USA
[9]Science Systems and Applications, Inc., Lanham, MD, USA

Correspondence: Jane Liu (janejj.liu@utoronto.ca)

Received: 19 March 2024 – Discussion started: 2 April 2024
Revised: 28 September 2024 – Accepted: 19 October 2024 – Published: 16 December 2024

Abstract. A global-scale horizontally and vertically resolved ozone climatology provides detailed insights into ozone variability. Here, the seasonal, annual and decadal monthly Trajectory-mapped Ozonesonde dataset for the Stratosphere and Troposphere (TOST) ozone climatology is improved and updated over 1970–2021. TOST is gridded at 5° × 5° × 1 km (latitude, longitude and altitude) from the surface to 26 km by the geometric coordinate and from the surface to 20 hPa at 26 pressure levels by the pressure coordinate, with the most recent ozonesonde data re-evaluated following the ASOPOS-2 guidelines (Smit and Thompson, 2021). Comparison between ozonesonde and trajectory-derived ozone shows good agreement for each decade, altitude and station, with relative differences (RDs) of 2 %–4 % in the troposphere and 0.5 % in the stratosphere. TOST also aligns well with aircraft, the Satellite Aerosol and Gas Experiment (SAGE) and the Microwave Limb Sounder (MLS) datasets. The updated TOST improves data coverage in all latitude bands and altitudes and reduces RD by 14 %–17 % compared to the previous version, taking advances in trajectory simulations and twice as many ozonesonde profiles. Higher uncertainties in TOST are where data are sparse, i.e., southern high latitudes, tropics and pre-1980s, and where variability is high, i.e., at the surface and upper troposphere–lower stratosphere (UTLS). Caution should therefore be taken when using TOST in these spaces and times. TOST captures global ozone distributions and temporal variations, showing an overall non-significant change in lower stratospheric ozone after 1998. TOST offers users a dataset with a long record, global coverage and high vertical resolution.

Published by Copernicus Publications on behalf of the European Geosciences Union.

1 Introduction

Ozone is an important oxidant photochemically linked to the hydroxyl radical in the troposphere, with detrimental effects on crop productivity, natural ecosystems and human health (Fleming et al., 2018; Harmens et al., 2018; Mills et al., 2018; Vicedo-Cabrera et al., 2020). Tropospheric ozone is the third-largest greenhouse gas contributing to radiative forcing, particularly in the upper troposphere (Gulev et al., 2021; Szopa et al., 2021; Forster et al., 2021). The global ozone distribution and its long-term changes at different altitudes, longitudes and latitudes are critical to understanding global ozone variability and its forcing on climate change. While the ozone trends themselves can indicate the impact of changes in climatic dynamics (Hassler et al., 2008) and chemistry, including the effect of the Montreal Protocol (Steinbrecht et al., 2017), long-term horizontally and vertically resolved ozone data are needed for prescribing, evaluating and refining ozone simulations in climate models (Hassler et al., 2018) and for quantifying changes in radiative forcing and projecting reliable future climate scenarios (Nowack et al., 2015).

Balloon-borne ozonesondes are the principal source of trend-quality long-term records of ozone profiles below ~ 18 km (Tarasick et al., 2021). In addition, lidar records also provide long-term tropospheric ozone profiles, such as the Observatoire de Haute-Provence lidar and the Jet Propulsion Laboratory Table Mountain lidar (Ancellet and Beekmann, 1997; McDermid et al., 2002). However, the horizontal coverage and temporal coverage of both ozonesondes and lidars are limited by the sparse distribution of the stations (less than 100 worldwide for ozonesondes and 9 lidars from the Tropospheric Ozone Lidar Network) and their low observation frequency (one to three times per week for ozonesondes; one to five times per week for lidars) (McDermid et al., 2002; Liu et al., 2013a; Chouza et al., 2019; Ancellet et al., 2022). The In-Service Aircraft for a Global Observing System (IAGOS) program has measured ozone profiles worldwide since 1994 via the instruments on board a number of commercial aircraft, with high sampling frequency at some airports (Thouret et al., 1998). However, sampling is unevenly distributed both spatially and temporally because the flights are constrained by commercial airlines' operation schedules. Satellite observations have the advantage of providing ozone data on a global scale with consistent quality. However, it is still challenging to retrieve tropospheric ozone through the large stratospheric ozone burden (Bhartia, 2002). Satellite data can provide total column ozone retrievals which are not yet vertically resolved. The satellite ozone profiles have limited vertical sensitivity, and the sensitivity decreases strongly toward the surface (Liu et al., 2010; Keppens et al., 2015). The direct retrieval from nadir-viewing instruments typically provides one to two pieces of independent information vertically in the troposphere (D. W. Tarasick et al., 2019). Large retrieval errors occur when retrieval sensitivity is low, as the solution relies heavily on the a priori profile (Keppens et al., 2015). In addition, single space instruments are of limited lifetime, while long-term studies on ozone require combining measurements from different instruments, which could introduce uncertainty related to the differences among different instruments (Rahpoe et al., 2015). A number of studies have developed long-term (since the 1980s) ozone climatologies by combining ozone measurements with ozonesondes and multiple satellite instruments (McPeters et al., 2007; McPeters and Labow, 2012; Hassler et al., 2018; Bodeker et al., 2021; Bognar et al., 2022), but these datasets are generally zonally averaged. Chemistry–climate models are also developed to provide ozone fields in three dimensions in latitude, longitude and altitude, especially for long-term and global-scale simulations (Eyring et al., 2010; Chen et al., 2018); these models present our best understanding of processes controlling ozone variations but still suffer from large uncertainties associated with emission inventories, parameterizations, radiation transport schemes and simulation of the atmospheric circulations (Young et al., 2018; Wild et al., 2020; Griffiths et al., 2021; Zeng et al., 2022). Some advanced models can improve global tropospheric ozone in three dimensions by assimilating the satellite data to enhance the modeling accuracy (Miyazaki et al., 2020a; Colombi et al., 2021). However, in addition to the aforementioned sources of uncertainties, such assimilations still rely heavily on the sufficiency and spatial–temporal continuity of the satellite data (Huijnen et al., 2020; Miyazaki et al., 2020b).

Liu et al. (2013a, b) constructed a long-term 3-dimensional global-scale ozone dataset using a trajectory-mapping approach, extending sparse ozonesonde measurements and filling gaps in the spatial domain with backward and forward trajectory simulations. The trajectory-mapping method assumes the ozone mixing ratio in the same air parcel along each trajectory is constant for several days, which is reasonable given that the lifetime of ozone in most of the troposphere and lower stratosphere ranges from days to months, varying with season and altitude (Han et al., 2019; Prather and Zhu, 2024). The constructed global dataset is independent of satellite measurements and photochemical modeling. The trajectory mapping can outperform conventional statistical interpolation methods (Stohl et al., 2001) because it is based on sound principles of ozone lifetime and wind-driven air movement. The trajectory-derived ozone data cover higher latitudes (to 90° N and 90° S) and a longer time period (since the 1960s) (Liu et al., 2013b). The Trajectory-mapped Ozonesonde dataset for the Stratosphere and Troposphere (TOST) version 1 (TOST-v1; Liu et al., 2013a, b) is available from 1965–2012 at the World Ozone and UV Data Centre (WOUDC; https://woudc.org/archive/products/ozone/vertical-ozone-profile/ozonesonde/1.0/tost/, last access: 28 September 2024). TOST was included in assessing tropospheric ozone column trends in the latest Intergovernmental Panel on Climate Change Sixth Assessment report (Gulev et al., 2021) and Tropospheric Ozone Assessment Re-

port (TOAR; Gaudel et al., 2018). It has also been used in studies of air quality and ozone–climate interactions (Polvani et al., 2017; Moeini et al., 2020; Griffiths et al., 2021). Because gaps remain in TOST data, for users' convenience, the gaps were filled, and all the data were smoothed with a linear combination of spherical functions, labeled and provided as smoothed data in TOST. Yet, the smoothed data should be used with caution; otherwise, misinterpretation of the smoothed data can be problematic (Chipperfield et al., 2022).

There have been several important developments since the publication of the first version of TOST data in 2013 (TOST-v1, Liu et al., 2013a, b). Constructing an improved version of TOST, namely TOST-v2, becomes necessary for the following reasons. Firstly, there are some 50 000 new ozone profiles, many from newly established ozonesonde stations (see Sect. 2.1). These new ozonesonde data permit an update of TOST, providing 3-dimensional ozone data with larger areal coverage and longer periods up to 2021. Secondly, data from many ozonesonde stations have been updated to higher-quality versions. An important source of uncertainty in TOST-v1 is possible biases in station records due to instrument changes and/or changes in operating procedures. Homogenized time series are now available from the Harmonization and Evaluation of Ground Based Instruments for Free Tropospheric Ozone Measurements (HEGIFTOM) project for over 40 ozonesonde stations (Table S1 in the Supplement). For these records, biases due to instrument changes, sensing solution and preparation changes have been corrected, to reduce the overall uncertainty from 10 %–20 % to 5 %–10 % (Smit and Thompson, 2021). This effort to improve data quality also uncovered an apparent change of bias at stations flying one type of sonde (Stauffer et al., 2020, 2022); 14 global ozonesonde stations (the bolded stations in Table S1) have shown an apparent drop-off of 2 %–4 % in stratospheric ozone and total ozone column since circa 2013, due to a possible instrument artifact. This is the subject of ongoing research (Tarasick et al., 2023). For these stations, ozone measurements above 40 hPa ($\sim$ 20 km) are not recommended for trend calculations. We need therefore to exclude data above 40 hPa for the affected profiles in constructing TOST. Thirdly, version 4.9 of the Hybrid Single-Particle Lagrangian Integrated Trajectory (HYSPLIT) model (Draxler and Hess, 1998) used for trajectory simulation has been improved and updated to version 5.2. Here, we address the mentioned issues and construct an improved and updated TOST using the most state-of-the-art HYSPLIT and the most updated ozonesonde data. Fourthly, while Liu et al. (2013a, b) validated TOST-v1 with ozonesonde data at 20 selected stations, TOST-v2 is validated against the ozonesonde data at all 141 stations individually with the trajectory-mapped approach omitting the input from the station being tested. In addition, comparisons are made with the IAGOS measurements in the troposphere and with two limb-viewing satellite measurements, the Satellite Aerosol and Gas Experiment (SAGE) and the Microwave Limb Sounder (MLS), in the stratosphere. This more comprehensive validation and the associated uncertainty analysis demonstrate the improved quality of TOST-v2 and also provide some caveats for users of TOST.

In the following, Sect. 2 describes the datasets, including ozonesonde, satellite and aircraft data and the trajectory-mapping methodology. Section 3 shows the validation results, comparisons with satellite and aircraft observations, a summary of uncertainties in TOST-v2, and improvements in TOST-v2. Based on TOST-v2, we characterize global ozone variations in the troposphere and stratosphere and show stagnant ozone variation in the lower stratosphere since the late 1990s in Sect. 4. Finally, conclusions are drawn in Sect. 5.

2 Data and methods

2.1 Ozonesonde data

Ozonesonde data over 1970–2021 at 141 ozonesonde stations worldwide (Fig. 1) were downloaded from the World Ozone and Ultraviolet Radiation Data Centre (WOUDC; https://woudc.org/archive/Archive-NewFormat/OzoneSonde_1.0_1/, last access: 4 December 2024) or, where available, homogenized data from Southern Hemisphere ADditional OZonesondes (SHADOZ; https://doi.org/10.57721/SHADOZ-V06) and HEGIFTOM (https://hegiftom.meteo.be/datasets/ozonesondes, last access: 28 September 2024). The homogenized ozonesonde stations from HEGIFTOM include ozonesonde stations from the SHADOZ network (Thompson et al., 2017; Witte et al., 2017, 2018), the Canadian network (Tarasick et al., 2016), the US network (Sterling et al., 2018), the Network for the Detection of Atmospheric Composition Change (NDACC) and several individual stations (Van Malderen et al., 2016; Witte et al., 2019; Ancellet et al., 2022), with an overall uncertainty of 3 %–5 % in both the stratosphere and troposphere. Ozonesonde data from the Beijing Nanjiao Meteorological Observatory (39.81° N, 116.47° E) in Beijing, China, are provided by the Institute of Atmospheric Physics (IAP), Chinese Academy of Sciences. The ozone profiles at Beijing are measured by the Brewer-Mast type GPSO3 ozonesonde and the IAP electrochemical concentration cell (ECC) ozonesonde, which are in fair agreement with commercial ECC ozonesondes (Wang et al., 2003; Xuan et al., 2004; Bian et al., 2007) in both laboratory and field experiments (Zhang et al., 2021; Zeng et al., 2023). In total, data from 43 more stations were used in TOST-v2 than in TOST-v1 (Liu et al., 2013b).

Figure 1a provides an overview of the distribution of the ozonesonde stations, the number of profiles and the beginning year for every station. Most of the stations with data before the 1980s are located in North America, Europe and east Asia. The majority of the stations in the Southern Hemisphere started measurement in the 1990s or later, and so the

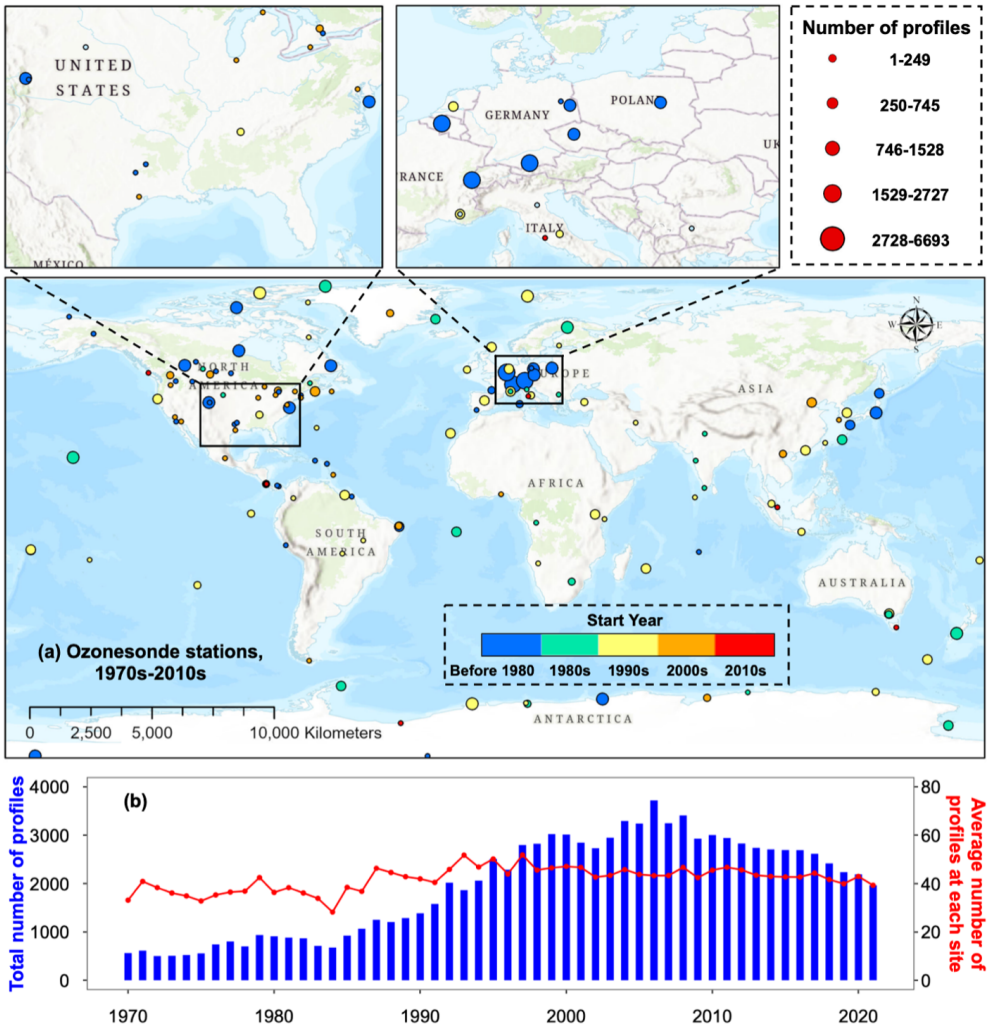

Figure 1. **(a)** Global distribution of ozonesonde stations used in this study to construct TOST-v2. Station details are provided in Table S1. The size and color of the dots indicate the total number of sounding profiles and the start year of the measurement time series. **(b)** The total number of profiles per year (left y axis, blue bars) and the average number of profiles per site and per year (right y axis, red dots and line) from 1970 to 2021.

Southern Hemisphere contains a smaller number of ozone profiles than in the Northern Hemisphere. Figure 1b shows that the total number of ozonesonde profiles per year has almost doubled since the 1990s and reached a maximum in the late 2000s, with over 3000 profiles per year. Since then, the number of ozonesonde profiles available on the WOUDC site has declined slightly to 2000–3000 profiles per year. The average annual number of profiles per station has slightly increased since the 1990s and has stabilized at about 40 profiles per year.

All the ozonesonde profiles were processed into 1 km vertical resolution by integrating and averaging the ozone mixing ratio in 1 km layers from the sea level. The ozonesonde data above 26 km were excluded as the data above this height show large uncertainties at midlatitudes and high latitudes (Fioletov et al., 2006).

2.2 Trajectory simulation

Forward and backward trajectories in 4 d were simulated every 6 h using the version 5.2 HYSPLIT model (Stein et al., 2015). HYSPLIT was driven by the reanalysis of hourly meteorological data from the National Centers for Environmental Prediction – National Center for Atmospheric Research (NCEP/NCAR), which has a horizontal resolution of 2.5° by 2.5° in latitude and longitude and 17 vertical levels from the surface to 10 hPa (Kalney et al., 1996). The length of the trajectories influences the spatial coverage and accuracy of the ozone mapping. Generally, uncertainties increase rapidly along the trajectories, with typical errors of about 100–200 km d^{-1} (Stohl, 1998). Trajectories have horizontal uncertainties of 350–400 km after 3 d and 600–1000 km after 4 d in the Northern Hemisphere (Engström and Magnusson, 2009). Trajectories show typical vertical deviations of about

200, 800 and 1000 m after 2, 4 and 6 d in the stratosphere and even greater uncertainties in the troposphere (Stohl and Seibert, 1998). Therefore, to limit trajectory errors, 4 d trajectories were used herein, following previous studies (Tarasick et al., 2010; Liu et al., 2013a, b).

2.3 Three-dimensional ozone mapping based on ozonesonde profiles and trajectories

Ozone mixing ratios from each sounding at the 26 levels were assigned to the corresponding forward and backward trajectory paths. These ozone values at positions every 6 h along the 4 d backward and forward trajectories (32 positions for each level for both forward and backward trajectories) were averaged in bins of 5° latitude and 5° longitude, for each 1 km altitude for every month. This bin size corresponds both to the typical uncertainties of 4 d trajectories discussed above and to the typical ozone correlation length (500–1500 km) in the troposphere and the stratosphere (Liu et al., 2009). To produce the mapping with pressure altitudes, we also averaged the 4 d backward and forward trajectories in bins of 5° latitude and 5° longitude for every month, using the pressure altitudes generated by HYSPLIT trajectories. The 26 pressure altitudes are 950, 850, 750, 650, 550, 450, 400, 350, 300, 250, 225, 200, 175, 150, 125, 100, 90, 80, 70, 60, 50, 40, 35, 30, 25 and 20 hPa, following the pressure coordinates in the European Centre for Medium-Range Weather Forecasts Reanalysis version 5 (ERA5). Ozonesonde profiles in both the troposphere and stratosphere were used. In addition, the ozonesonde data at the 26 levels are separated into the troposphere and stratosphere from the measured ozonesonde temperature profile, following the World Meteorological Organization (WMO) definition of the tropopause. In this way, two datasets are constructed using ozonesonde data in the troposphere (troposphere-only) and in the stratosphere (stratosphere-only). The troposphere-only and stratosphere-only fields are helpful to calculate the tropopause in modeling studies, as the average tropopause height is usually not specified in the full-atmosphere field.

Based on this mapping, TOST-v2 was constructed at 26 altitude levels in two altitude coordinates (by geometric levels and pressure levels), from two altitude starting levels (altitude above sea level and altitude above ground level), for three temporal resolutions (in the seasonal mean for each year, the annual means for each year from 1970 to 2021 and monthly means for each decade from the 1970s to the 2010s) and with three types of data fields (trop-stra, troposphere-only and stratosphere-only) for users' convenience (Table 1). In TOST-v2, we also generated the corresponding datasets that show ozone variation at three percentile levels (25, 50 and 75th). Examples presented in this paper all use TOST at geometric coordinates with altitudes above sea level. For this coordinate system, both ozonesonde profiles and mapped data necessarily begin at the altitude of the surface, leaving the levels below the topography of the Earth's surface as null if the levels are above the sea level.

Errors in the mapped data can come from trajectory errors and from ignoring ozone chemistry (production and loss) along the transport pathway and deposition in the surface layer (Liu et al., 2013a). Differences between the results of backward and forward trajectory mapping can provide a measure of these errors, since in the absence of such errors the results of forward-only and backward-only trajectory mapping should be identical. Therefore, mappings from the forward-only and backward-only trajectories were compared as an initial quality check. Figure S1 in the Supplement shows monthly means (January and July) in 2000 at 3–4 and 19–20 km, for forward-only and backward-only mapping. In general, the differences between the two mappings are commonly less than 15 % and have no distinct pattern, indicating that trajectory errors are not dependent on the direction of the trajectories. These modest differences between forward-only and backward-only trajectory-mapped ozone fields also validate the reliability of this trajectory-mapping method; both backward and forward trajectories, therefore, were combined in TOST to achieve better averages and higher spatial coverage.

2.4 Validations of TOST

To comprehensively validate TOST, we compare TOST with actual ozonesonde, satellite, and aircraft observations. Multiple metrics were used to indicate the level of agreement between the TOST and other data. We used the correlation coefficient (R) to present the agreement of the two compared data, and linear fitting coefficient with the intercept set to 0 to show the overall tendency of overestimation or underestimation. We also used relative difference (RD) to represent the relative difference between the two compared data and used bias and root mean square difference (RMSD) to show the absolute difference between the two compared data. Details of the metrics can be found in Sect. S1 in the Supplement.

2.4.1 Ozonesonde profiles for validation

We first validate TOST by comparing the actual ozone profile at each of the ozonesonde stations with the trajectory-derived ozone profile for that station without the input of that station itself. This method is computationally intensive, as the trajectory mapping must be re-calculated (with data for all stations except one), for each ozonesonde station, but it directly tests the reliability of deriving ozone concentrations at a location by integrating the contributions via trajectories from surrounding sites, which is the essential assumption of the trajectory-mapping method. We refer to this set of data that selectively excludes the local data at each station as "Traj-derived" throughout this paper.

Table 1. The description of the classifiers and the corresponding types for the TOST data.

Classifier	Type	Description
1. Vertical coordinate	Geometric	Altitude coordinates are 1, 2, . . . , 25 and 26 km at 1 km vertical resolution.
	Pressure	Altitude coordinates are 950, 850, 750, 650, 550, 450, 400, 350, 300, 250, 225, 200, 175, 150, 125, 100, 90, 80, 70, 60, 50, 40, 35, 30, 25 and 20 hPa.
2. Starting level	Sea-level	Data start at the altitude of the sea surface. Ozone value for levels beneath the topography of the Earth's surface is set to null.
	Ground-level	Data start at the altitude of the ground surface.
3. Temporal resolution	Seasonal	Data are the mean for each season of the year (1970–2021).
	Annual	Data are the annual mean for each year (from 1970–2021). Each grid requires at least one value per season to be included in the annual data.
	Decadal-monthly	Data are the monthly mean for each month of a decade (from the 1970s to 2010s).
4. Ozonesonde data used	Trop-stra	Data are based on ozonesonde profiles in both the troposphere and stratosphere. This is the main dataset of TOST.
	Troposphere-only	Data are based on ozonesonde profiles only in the troposphere.
	Stratosphere-only	Data are based on ozonesonde profiles only in the stratosphere.
5. Ozone variation	Mean	The mean ozone concentrations for each grid cell over a period (a month, a year or a month of a decade).
	25th, 50th and 75th percentiles	The 25th, 50th and 75th percentiles of ozone concentrations for each grid cell over a period (a month, a year or a month of a decade). Only available for trop-stra data.
6. Supplement data	Smoothed data	Smoothed ozone fields by fitting the maps at each level with a linear combination of spherical functions.
	N	The total number of samples for each grid cell.
	N of independent samples	The total number of trajectories passed for each grid cell. A trajectory is counted only once in a grid cell when the trajectory passes that cell regardless of how long the trajectory stays in that cell.
	SD	The standard deviation for each grid cell.
	CV(SD/mean)	The CV for each grid cell.
	SE	The standard error for each grid cell.
	SE/mean	The ratio of the standard error to the mean for each grid cell.

2.4.2 Satellite ozone profile for comparison with TOST in the stratosphere

TOST is further compared with two well-known satellite limb sounder datasets, the Satellite Aerosol and Gas Experiment (SAGE) and the Microwave Limb Sounder (MLS).

SAGE II was launched into a 57° inclination orbit on board Earth Radiation Budget Satellite (ERBS) and was in operation from 1984–2005. Using the highly accurate solar occultation technique, SAGE can resolve ozone vertical variation in the stratosphere and the middle–upper troposphere at 1 km vertical resolution (Kent et al., 1993), with the highest accuracy over the 20–45 altitudes (Cunnold et al., 1996). Here we use the version 7.0 SAGE II ozone mixing ratio (https://sage.nasa.gov/missions/about-sage-ii/, last access: 28 September 2024) in the 1980s and 1990s for the comparison.

The MLS, on board the Aura satellite, can measure stratospheric ozone profiles with a vertical resolution of about 3 km. MLS observes microwave radiances that are both emitted and absorbed by the atmosphere. The retrieval is more complex and uses the optimal estimation approach. Here we use the version 5.0 MLS ozone mixing ratio (https://disc.gsfc.nasa.gov/datasets/ML2O3_005/summary?keywords=ML2O3_005, last access: 28 September 2024) in the 2000s and 2010s for the comparison.

2.4.3 Aircraft ozone profiles for comparison with TOST in the troposphere

The IAGOS network (https://www.iagos.org/, last access: 28 September 2024) has been measuring ozone profiles worldwide since 1994 via dual-beam ultraviolet absorption monitors on board commercial aircraft (Petzold et al., 2015), with an accuracy of about $\pm$ (2 nmol mol^{-1} +2 %) (Nédélec et al., 2015). Ozone monitors are calibrated annually to a reference analyzer at the Bureau Internationale des Poids et Mesures (BIPM) and also compared every 2 h to an in-flight ozone calibration source. Generally good agreement is found between IAGOS profiles and ozonesondes, with positive biases for the sondes of 5 %–10 % (Tilmes et al., 2012; Zbinden et al., 2013; Staufer et al., 2013, 2014; Tanimoto et al., 2015; D. W. Tarasick et al., 2019), making IAGOS ozone suitable for the validation of TOST. Here, the IAGOS ozone profiles were processed into 1 km layers from sea level and averaged into bins of 5° latitude and 5° longitude for each month. In total, all IAGOS ozone data from 310 airports were used for the comparison (Table S2). Then, the processed IAGOS ozone profiles were matched with the TOST ozone for the corresponding grids to examine the performance of TOST in the troposphere.

3 Validations and comparisons of TOST

3.1 Validations with ozonesonde observations

First, we show the overall comparison in monthly mean ozone concentrations between ozonesonde and trajectory-derived values without the inputs of the stations being tested (Traj-Derived), from all the existing stations at all altitude levels. Note that the actual TOST dataset would be better than "Traj-Derived ozone", especially at the sampling locations because the input of the local station is included in the TOST dataset. Because of the large range of ozone concentrations in the troposphere and stratosphere (0–6000 ppb), we divide the altitude levels into three to present the overall accuracy of TOST in the lower troposphere (ozone concentrations below 50 ppb), the upper troposphere (ozone concentrations between 50 and 150 ppb) and the stratosphere (ozone concentrations over 150 ppb).

Figure 2a–f show the overall ozone comparisons between ozonesonde (Sonde-Observed) and Traj-Derived ozone in the entire study period (Fig. 2a–c) and each decade (Fig. 2d–f). Each dot in Fig. 2a–c represents the paired ozone concentrations from Traj-Derived and Sonde-Observed values in each month at each latitude–longitude–altitude grid cell, and the color indicates the density of the dots. Overall, in the lower troposphere (Fig. 2a), the Sonde-Observed and Traj-Derived ozone concentrations agree well, with an R of 0.69 and an RMSD of 7.5 ppb, a low bias (0.7 ppb) and a low RD (1.8 %). The linear fit for the entire study period shows a slope of 0.99. In the upper troposphere (Fig. 2b), the agreement between the Sonde-Observed and Traj-Derived ozone concentration is moderately lower, with a linear fitting coefficient of 1.01 and RMSD of 21.1 ppb, and higher bias (2.9 ppb) and RD (4.0 %) than those in the lower troposphere. This lower agreement in the upper troposphere is owed to the greater influence of stratosphere–troposphere exchange (STE) in the upper troposphere, where trajectories by the Lagrangian dispersion model (such as HYSPLIT) show substantially increased deviations due to the strong turbulence and convection (Stohl et al., 2002). The positive bias may imply that STE is slightly overestimated in HYSPLIT. In the stratosphere (Fig. 2c), the overall agreement between the Sonde-Observed and Traj-Derived ozone concentrations has a linear fitting coefficient of 0.97 and an RMSD of 416.9 ppb. The RD is only 0.5 %, indicating higher reliability of Traj-Derived in the stratosphere.

This validation method compares ozonesonde station data with Traj-Derived ozone, i.e., the ozone found by averaging trajectories that come from other stations. Before the 1990s, RDs were smaller than 0 and R values were smaller than 0.60 (Fig. 2d and e) in the lower troposphere, indicating a tendency to underestimate the Traj-Derived ozone in the lower troposphere. After the 1990s, owing to the additional ozonesonde measurements provided by SHADOZ in the tropics, the underestimation of Traj-Derived ozone in the

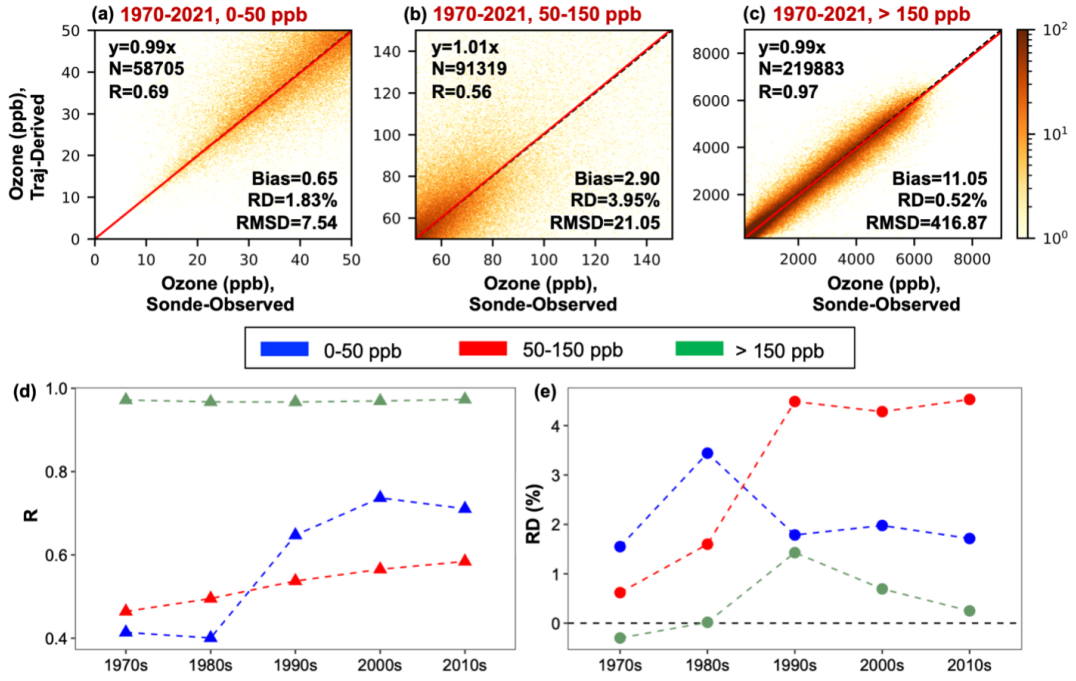

Figure 2. **(a–c)** Comparison of monthly mean tropospheric ozone mixing ratios from ozonesondes (Sonde-Observed) and trajectory-derived TOST data (Traj-Derived) for the study period at 0–50, 50–150 and > 150 ppb. Solid red lines represent the linear fitting line (with the intercept set to 0), and dashed black lines denote the 1 : 1 axis. N is the total number of data points, R is the correlation coefficient, bias is the overall average difference in monthly means (Traj-Derived ozone − Sonde-Observed ozone; in ppb), RD is the relative difference (in %) (100× (Traj-Derived ozone − Sonde-Observed ozone) / Sonde-Observed ozone), and RMSD is the root mean square difference (in ppb). Note that Traj-Derived ozone at each station is derived without input from the station itself; that is, Traj-Derived represents an ensemble of 141 separate computations of TOST, each one withholding a single validation station. **(d–e)** The R and RD between the Traj-Derived ozone and Sonde-Observed ozone by decade. The dashed black line in **(e)** denotes where the RD is 0.

lower troposphere is greatly reduced, and the R value increases to > 0.71 (Fig. 2d and e). Similarly, with the additional ozonesonde measurements after the 1990s, the R values in the upper troposphere increased from < 0.50 to > 0.58 (Fig. 2d). In all decades, the agreement between Sonde-Observed and Traj-Derived ozone in the stratosphere is the best, with an R value of ∼ 0.97. The RD in each decade is small (−0.3 %–1.4 %), indicating no systematic underestimation or overestimation in the stratospheric Traj-Derived data. However, in the upper troposphere, ozone concentrations are slightly overestimated by Traj-Derived ozone data concentrations, with RD of 0.6 %–4.5 %.

Figure 3 examines how the RD between the ozonesondes and Traj-Derived ozone values varies with altitude, presenting the frequency distributions of RD across all stations, at every other altitude level and in each decade. The RD distributions are based on the monthly ozone concentration difference between the actual ozonesonde and Traj-Derived data from all the existing stations at the corresponding altitude level and decade. The distributions of RD show little skewness in these altitudes and decades, indicating no systematic bias during the study period. The overall interquartile ranges (25–75th), denoted by thick red lines with the widths given in red values, indicate that RD is between −30 % to 30 % and the widths of interquartile ranges are between 9 % and 61 %, with the lowest interquartile ranges (−10 % to 10 %) and widths (9 % to 30 %) of RD in the stratosphere and lower–middle troposphere. Higher interquartile ranges of RD appear in the 13–19 km altitude range, where the upper troposphere–lower stratosphere (UTLS) region is located, and are due to the large vertical gradients of ozone concentrations in the UTLS and the variability of the tropopause (Millán et al., 2023). The surface (boundary layer) ozone, however, shows a positive bias of the median of up to 12 %, in all decades, suggesting that TOST, which neglects ozone chemistry and deposition processes, tends to overestimate ozone concentrations there.

Figure 4 exemplifies comparisons in vertical profiles between Sonde-Observed and Traj-Derived ozone profiles at individual stations in different seasons. Four stations with sufficient data coverage (> 15 years) were selected from the Antarctic coastal region (Syowa), Europe (Hohenpeissenberg), North America (Boulder) and east Asia (Beijing). The decadal-mean (1990s and 2000s) profiles in January and July are used to compare the performance of Traj-Derived ozone profiles in boreal winter and summer. In general, the

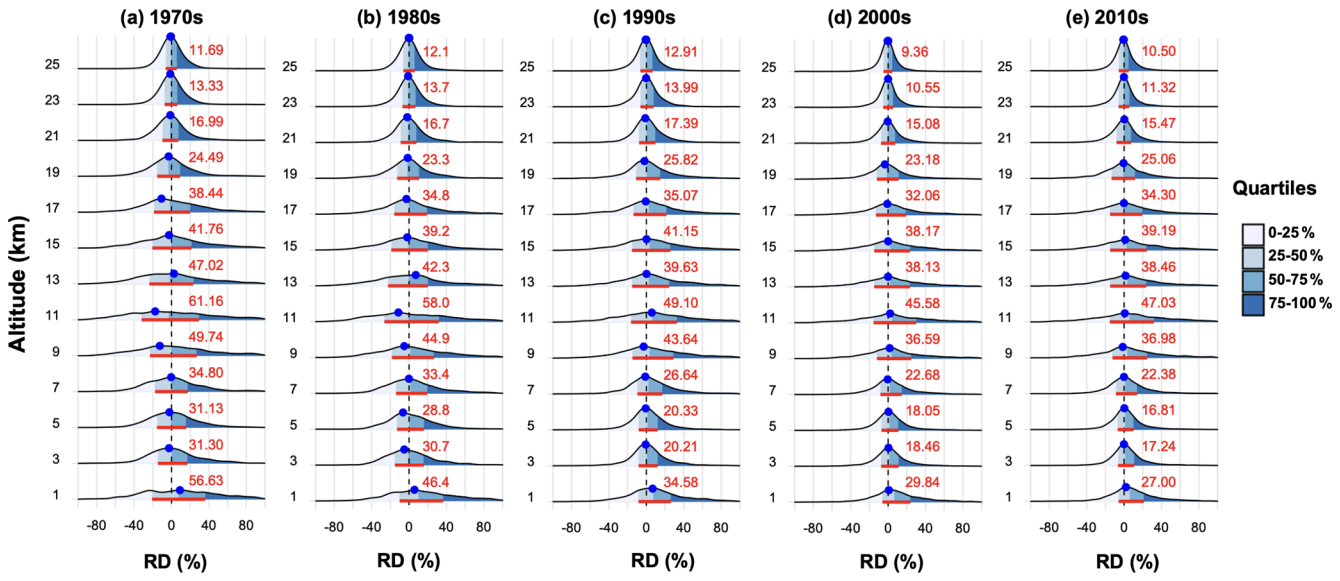

Figure 3. Frequency distribution of relative difference (RD) of the monthly ozone mixing ratios between ozonesonde and Traj-Derived data by every other altitude in the 1970s, 1980s, 1990s, 2000s and 2010s (y axis: frequency in %, x axis: RD in %), with the colors denoting the four quartiles of RD. The dashed line indicates zero difference in RD. The blue dot represents the maximum frequency. The thick red line denotes the width of distribution at 25–75 percentile, with the corresponding width of the distribution value in red.

Traj-Derived profiles can capture the vertical ozone variation in different seasons, with good correlation ($R > 0.99$) and high accuracy (bias < 100 ppb, RD < 10 %) in comparison to the actual ozonesonde profiles. The comparison at Syowa shows a larger bias, but much of this is due to the fact that in the 1990s this station launched the Japanese KC-79 carbon-iodine sonde, while other stations in the Southern Hemisphere launched ECC sondes; the Traj-Derived profiles would therefore be expected to be 10 %–20 % higher in the troposphere and about 5 % higher in the lower stratosphere (Smit and Kley, 1998). The excellent agreement in tropospheric ozone at Hohenpeissenberg is likely due to frequent and dense European ozonesonde observations; similar cases also are seen at Uccle, Payerne and Praha. Larger discrepancies are shown near the planetary boundary layer (PBL) and UTLS, as the simulated trajectories over these regions have more uncertainties (Stohl and Seibert, 1998; Sicard et al., 2019), and ozone chemistry and deposition are potentially important in the PBL at timescales similar to those of the longer trajectories (4 d) (Prather et al., 2023; Prather and Zhu, 2024).

3.2 Comparisons with satellite observations in the stratosphere

To compare with satellite data, we first validated the Traj-Derived ozone profiles against ozonesonde measurements. The corresponding validation was conducted for the satellite data of SAGE and MLS for the same period, location and altitude. The sets of ozonesonde, Traj-Derived and satellite data were selected only when all three datasets were available for the same month, decade and grid cell, to ensure that both the Traj-Derived and satellite data could be independently evaluated by the ozonesondes. As MLS data at altitudes below 261 hPa are not recommended (Livesey et al., 2022), we only compare both satellite datasets above this altitude, i.e., $\sim$ 16–26 km. Figure 5 shows the time series of the vertical variation of monthly RD from 16–26 km between Traj-Derived and SAGE ozone profiles from 1985–2005 (Fig. 5c and f) and between Traj-Derived and MLS ozone from 2005–2019 (Fig. 5i and l). SAGE ozone data are reliable above 20 km (Kremser et al., 2020), having a mean RD of about -10 %–10 % above this altitude, similar to that of Traj-Derived ozone. Between 16 and 20 km, SAGE ozone concentrations are lower than the Traj-Derived ozone by 5 % to 10 % (Fig. 5f), as Traj-Derived ozone overestimates the ozonesondes by 9 % to 15 % (Fig. 5e). Over the MLS period from 2005 to 2019, TOST ozone at all altitudes between 16 and 26 km agrees with actual ozonesondes better than during the SAGE period (Fig. 5h and k vs. Fig. 5b and e). Accordingly, the Traj-Derived ozone concentrations show good agreement with MLS ozone above 22 km but are lower than MLS ozone below 20 km (Fig. 5i and l), as MLS generally overestimates ozone concentrations below 20 km (Fig. 5g and j).

Figure S3 compares the RMSD of Traj-Derived and satellite ozone in different latitude zones from 16–26 km. Compared to SAGE in the 1990s, the Traj-Derived ozone has comparable RMSDs in the Northern Hemisphere, yet higher RMSDs in the Southern Hemisphere, due to the fewer ozonesonde stations there. MLS ozone also shows lower

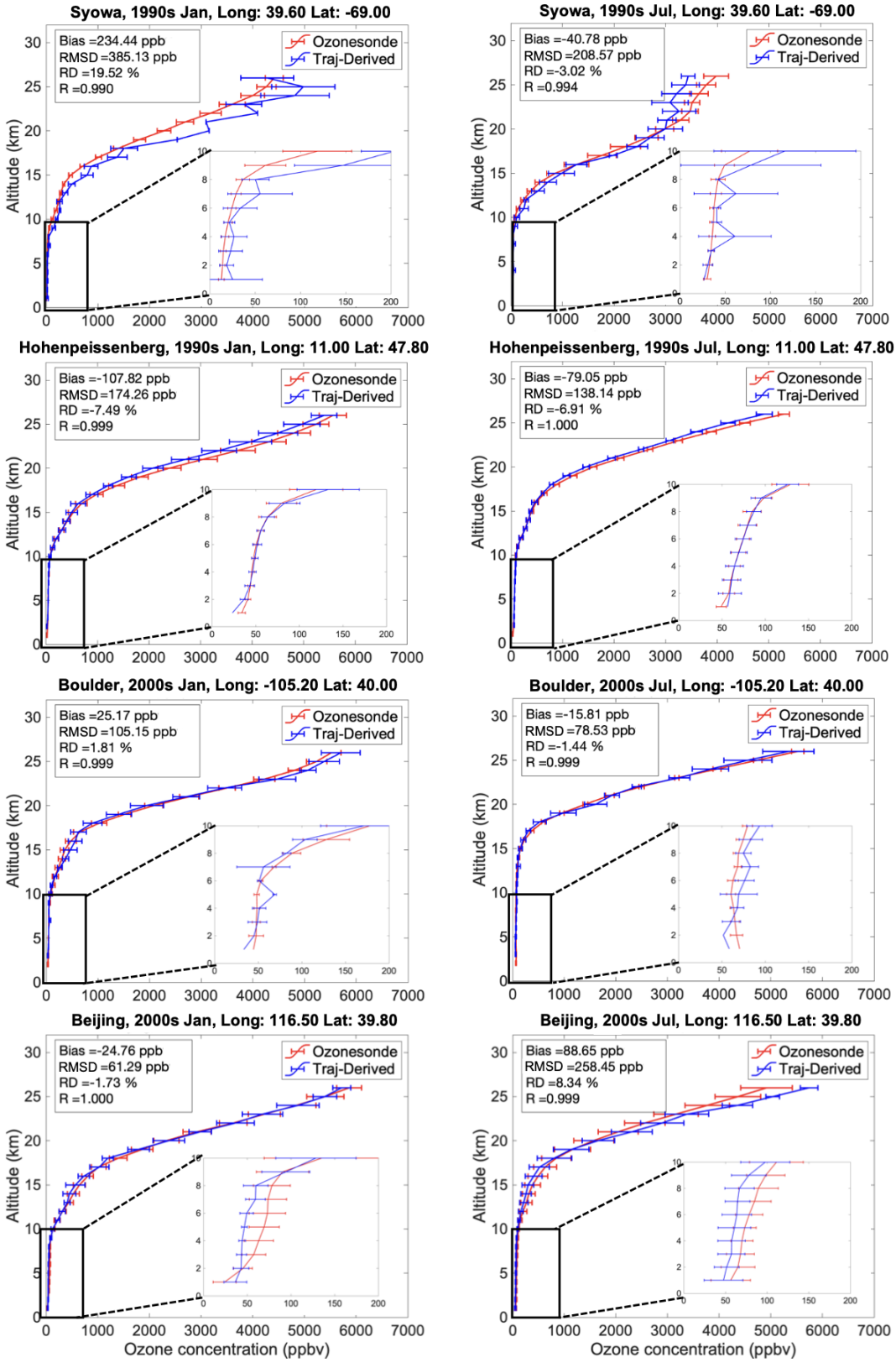

Figure 4. Decadal monthly mean ozone profiles at Syowa and Hohenpeissenberg in January and July of the 1990s and at Boulder and Beijing in January and July of the 2000s. The red line denotes ozonesonde ozone, and the blue line denotes trajectory-derived ozone without the input from the station itself. The error bar is ±2 times the standard error of the mean (equivalent to 95 % confidence limits on the averages). To better compare the difference of ozone profiles in the troposphere, a zoomed-in window from 0–10 km is provided in each sub-figure.

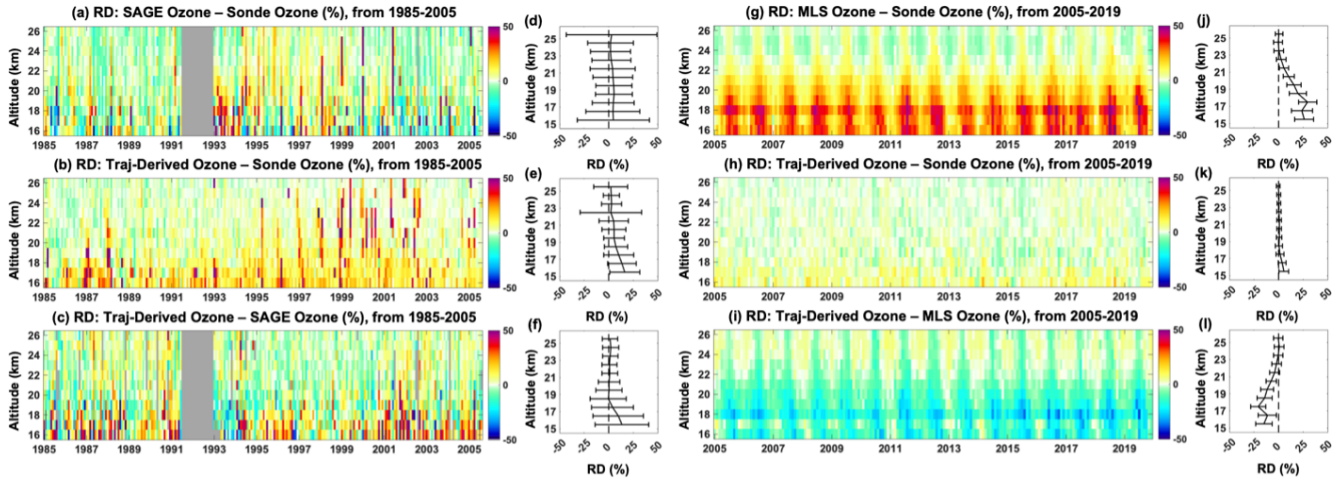

Figure 5. **(a)** The relative difference (RD) between ozonesonde and SAGE ozone data in each month and at each altitude during 1985–2005 over 16–26 km (RD = 100× (SAGE ozone − ozonesonde ozone) / ozonesonde ozone; in %). The mean RD over 1985–2005 at each level is shown on the right **(d)**, where the error bars represent the standard deviation of the monthly RD over 1985–2005. Note that the Pinatubo-affected SAGE profiles are excluded during July 1991–December 1992 (filled with gray color). **(b)** the same as **(a)**, but for the RD between ozonesondes and Traj-derived data (RD = 100× (Traj-derived ozone − ozonesonde ozone) / ozonesonde ozone; in %). **(c)** the same as **(a)**, but for the RD between Traj-derived and SAGE ozone data (RD = 100× (Traj-derived ozone − SAGE ozone) / (0.5× Traj-derived ozone +0.5× SAGE ozone); in %). **(d–f)** The averaged RD by altitude corresponding to **(a–c)**. **(g–l)** The same as **(a–f)** but for the period of 2005–2019, and the satellite measurements are from MLS ozone.

RMSDs in the Southern Hemisphere, but higher RMSDs in the Northern Hemisphere.

Table S3 summarizes the evaluation of both Traj-Derived and satellite ozone against the ozonesondes over 16–26 km. The Traj-Derived and SAGE ozone values show a high correlation ($R = 0.95$ or greater in all cases) with actual ozonesondes. The Traj-Derived ozone data show RDs of −1 % to +2 % in the 1980s and 1990s and just −0.3 % to +0.4 % in the 2000s and 2010s, while the SAGE ozone data show RDs of −4 % to +0.5 %, and the MLS data show RDs of −2 % to +11 %.

It is expected that TOST would outperform satellite instruments in measurements below the tropopause, as satellite measurements are hampered by the large stratospheric ozone burden that satellite instruments must look through. Yet, our comparisons suggest that even above 15 km, where SAGE and MLS are considered most reliable (Wang et al., 2002; Kremser et al., 2020; Livesey et al., 2022), TOST can provide comparable or better accuracy.

3.3 Comparisons with aircraft observations in the troposphere

We compare TOST ozone with the IAGOS dataset in the lower troposphere from 1994–2021 (Fig. 6). Note that this comparison is between the full TOST (not Traj-derived) and IAGOS datasets here. TOST ozone values are generally higher than IAGOS with a mean bias of 2.2 ppb and R of 0.49, but RDs (5.8 %) and RMSD (8.8 ppb) are low. The linear fit has a slope of 1.03. The two ozone datasets employ different measurement techniques and atmospheric sampling (Petetin et al., 2018). Previous studies have reported that IAGOS ozone values are systematically lower than ozonesonde values, typically by 5 %–10 % in the troposphere (Tilmes et al., 2012; Zbinden et al., 2013; Staufer et al., 2013, 2014; Tanimoto et al., 2015; D. W. Tarasick et al., 2019). The comparisons in Fig. 6 are consistent with these earlier estimates, as the RD indicates that IAGOS measurements average 6 % lower than TOST.

3.4 Uncertainty analysis

As noted in Sect. 2.3, the ozone concentrations in a grid in a month are determined by the ozone concentrations along all the trajectories passing through that grid cell in that month. Therefore, an estimate of the random uncertainty of TOST may be obtained from the standard error of the mean in each grid cell. Note that this may not be a true estimate of the standard error, as some cells may contain more than one value from an individual trajectory, so these values are not independent and the standard error calculation is biased low.

For convenience, given the large range of ozone concentrations between the stratosphere and troposphere, we use the ratio of the standard error to the mean in each of the grid cells, SE/mean (expressed in %), to estimate spatial patterns of the uncertainty. The standard error is proportional to the variability of the ozone values in a grid cell (i.e., the standard deviation) and inversely proportional to the square root of the number of data values. Thus in general, the more trajectories passing a grid cell, the more data samples for that cell and

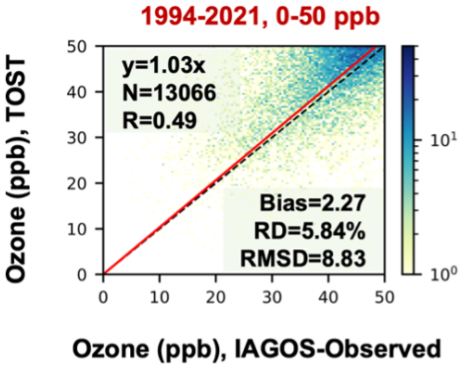

Figure 6. The comparison of monthly ozone mixing ratios between IAGOS-observed (x axis, labeled IAGOS-Observed) and TOST data (y axis, labeled TOST) from 1994–2021 for ozone concentrations below 50 ppb. Solid red lines represent the linear fitting line (with the intercept set to 0), and dashed black lines denote the 1 : 1 axis. N is the total number of data points, R is the correlation coefficient (unitless), bias is the difference in monthly mean values (TOST ozone – IAGOS ozone, unit: ppb), RD is the relative difference (100× (TOST ozone − IAGOS ozone) / (0.5× TOST ozone +0.5× IAGOS ozone)) and RMSD is the root mean square difference (unit: ppb).

the lower the standard error for that cell. For each cell, we also calculated the number of independent samples; i.e., the trajectory originated from a single ozonesonde altitude was counted only once in a grid cell when the trajectory passes that cell regardless of how long the trajectory stays in that cell. Figure 7 shows the SE/mean and the number of independent samples in January and July of the 2000s at 3–4 and 19–20 km. Generally, the Southern Hemisphere shows higher SE/mean values (> 10 %) than the Northern Hemisphere (< 6 %), which reflects the large number (> 100) of ozone soundings in the Northern Hemisphere, especially over North America and Europe. However, near the Equator, despite the higher sampling rate, the SE/mean is still as high as 15 %. Compared to the stratospheric level (19–20 km), the tropospheric level (3–4 km) shows an overall higher SE/mean. SE/mean varies less with season in the stratosphere than in the troposphere. For example, at 3–4 km, the SE/mean in January is generally < 7 % but becomes > 10 % in July in the Northern Hemisphere, and vice versa in the Southern Hemisphere. This is likely due to more vertical motion in the PBL (Stohl and Seibert, 1998; Sicard et al., 2019) so that ozone in some bins comes from multiple altitude levels, as well as increased photochemistry and biomass burning. Stratospheric intrusions to the lower troposphere are more frequent in boreal spring and summer than in winter (Terao et al., 2008; Greenslade et al., 2017) and can be responsible for much of the variability at 3–4 km (D. Tarasick et al., 2019).

To provide an overview of the uncertainties of TOST in different altitudinal and latitudinal zones, as well as in different seasons and decades, we calculated the RD of the monthly ozone mixing ratio between ozonesonde and Traj-Derived ozone over 1970–2021 (Fig. 8). Among altitudes, the highest RD values appear at 9–10 km over the tropopause region, and the second highest RD at the surface, while the lowest RD values are in the lower–middle troposphere (3–6 km) and stratosphere (19–26 km), consistent with Fig. 3. By season (Fig. 8b), the RD varies slightly with a lower value in JJA and SON than in other seasons. There is considerable variation in RDs with latitude (Fig. 8c); the RDs in the southern high latitudes (9–60° S) and the northern tropics (0–30° N) are higher than in other latitudinal zones. This could reflect higher horizontal gradients of ozone (e.g., stations in or outside the ozone hole) in the southern high latitudes or biases between ECC sondes and other types (the Indian and Japanese sondes) in the northern tropics. After the 1990s, the RDs are reduced markedly compared to the 1980s and 1970s (Fig. 8d), likely related to the improved data coverage in the later periods. This overview provides caveats regarding where (surface and UTLS, the northern high latitudes and tropics) and when (before the 1990s) more caution is advised when using TOST.

3.5 Improvements in the new version

The improvements in TOST-v2 are attributed to the increased amount and improved quality of ozonesonde data, as well as the improved trajectory simulation and ozone mapping. Because more ozonesonde stations and more ozonesonde data have become available since the 1990s or 2000s (Table S1), more ozone profiles were used in constructing TOST-v2, leading to improved data density. Table S4 summarizes the data coverage, the number of ozonesonde stations and the number of ozonesonde profiles used for TOST-v2 and TOST-v1. The data coverage is defined as the ratio of the number of grid cells with valid annual means to the total number of grid cells in the corresponding latitudinal zone. The number of ozonesonde stations, compared to Liu et al. (2013b), increases in all latitudes by ∼ 50 %, and the total number of ozonesonde profiles used is doubled. Data coverage increases as well, in all latitude bands, by 5 %–15 % (Table S4) and in all altitudes by a maximum of 10 % (Fig. S4).

In addition to the data density, the data quality was also improved in TOST-v2. Figure 9a–b show the distributions of ozone concentrations in TOST-v2 and TOST-v1 at the lowest level (0–1 km) for the 2000s. Over the Antarctic, gaps are observed only in TOST-v2. This is more reasonable for the sea-level data because the altitude over the Antarctic is over 1 km (Fig. S5a), where trajectories should not appear at 0–1 km. Therefore, the spatial distributions of ozone are clearly improved with this topography correction in TOST-v2, which could be attributed to the updated terrain file since HYSPLIT v5.0 (https://www.arl.noaa.gov/hysplit/hysplit-model-updates/, last access: 4 December 2024). Over the eastern Pacific, marked with an ellipse in Fig. 9a and b, TOST-v1 shows higher ozone concentrations than TOST-v2

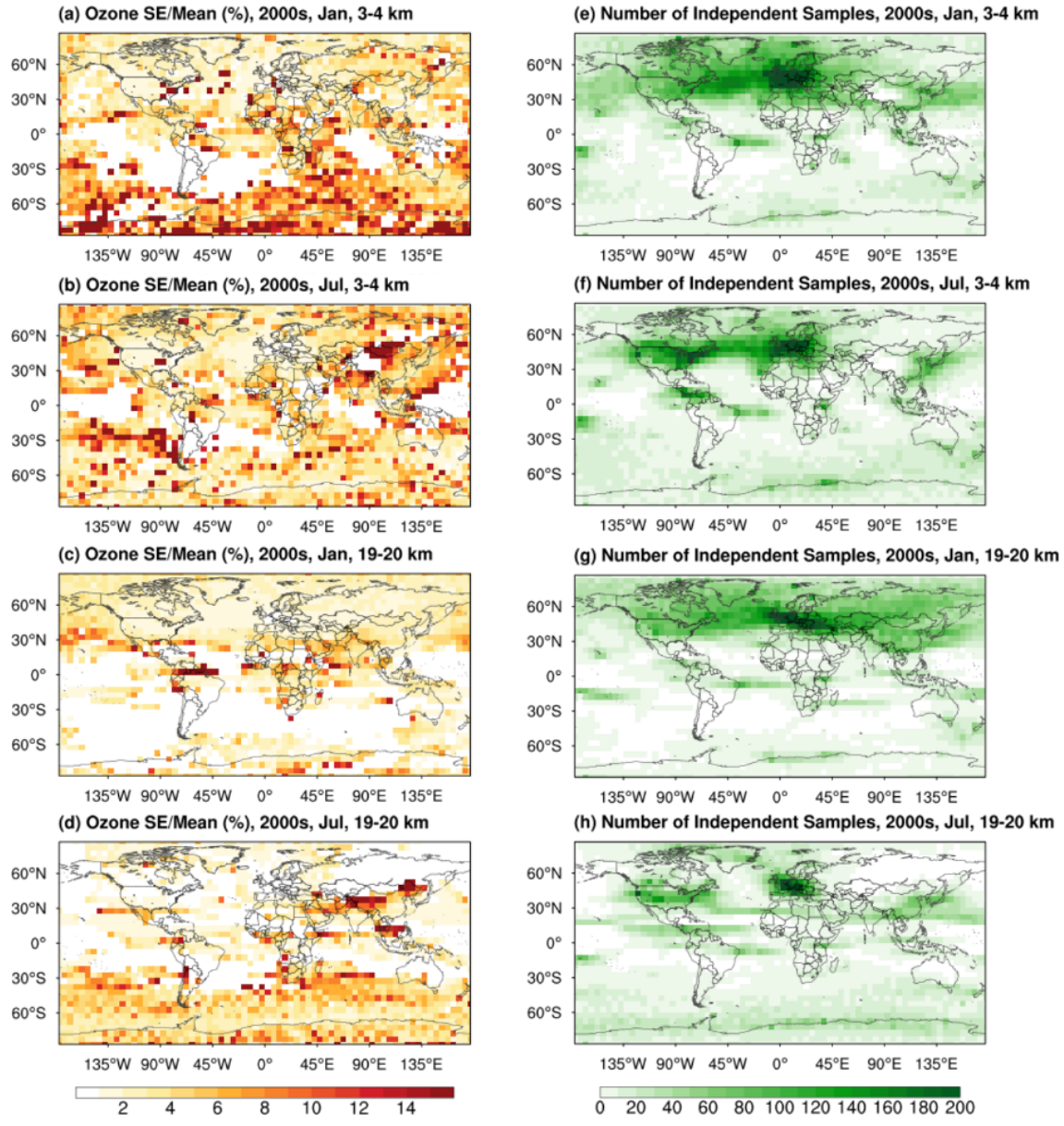

Figure 7. **(a–d)** Global distribution of the SE/mean (left panels, in %) for the decadal monthly mean ozone in January and July 2000s at 3–4 km **(a, b)** and 19–20 km **(c, d)**. **(e–h)** The same as **(a–d)** but for the number of independent samples in each 5 × 5° bin.

by 30 % (Fig. 9c). Compared to the ozonesonde measurement at 0–1 km in the 2000s in these two regions (Davis station for the Antarctic and Easter Island station for the eastern Pacific), TOST-v2 agrees better with ozonesondes than TOST-v1, indicating better representation of ozone distributions (Fig. S5b).

With reference to spatial distributions at 19–20 km in the 2000s, Fig. 9d–e show that in the Antarctic and the tropical eastern Pacific, TOST-v1 values show higher concentrations than TOST-v2 (Fig. 9f). Figure S5c compares ozone concentrations from ozonesonde, TOST-v2 and TOST-v1 at 19–20 km in the 2000s at an Antarctic station (Syowa) and a tropical station (Bogotá). Compared to TOST-v1, TOST-v2 ozone values show a better agreement with the ozonesonde measurement. The difference between TOST-v2 ozone and ozonesonde measurements is 10 % and 29 % in Syowa and Bogotá stations, while in TOST-v1, ozone concentrations at these stations show 24 % and 39 % differences (Fig. S5c).

In summary, TOST has been improved in TOST-v2 with higher spatial coverage, improved description of ozone spatial distributions and a better agreement with ozonesonde measurements in both the troposphere and stratosphere. Furthermore, TOST-v2 provides additional information that shows ozone variations in three percentile levels (25, 50 and

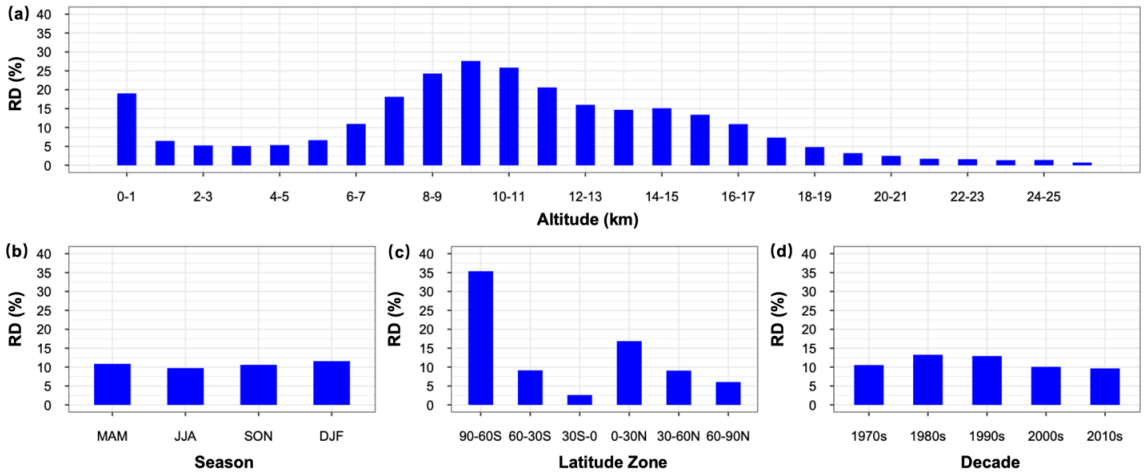

Figure 8. The RDs (in %) of TOST over 1990–2021 by altitude **(a)**, and the average RDs over all altitudes by season (MAM (March–April–May), JJA (June–July–August), SON (September–October–November) and DJF (December–January–February)) **(b)**, latitudinal zone **(c)** and decade **(d)**. RD is calculated by the mean ozone mixing ratio from Traj-Derived ozone and ozonesondes measurements (100× (Traj-Derived ozone − Sonde-Observed ozone) / Sonde-Observed ozone).

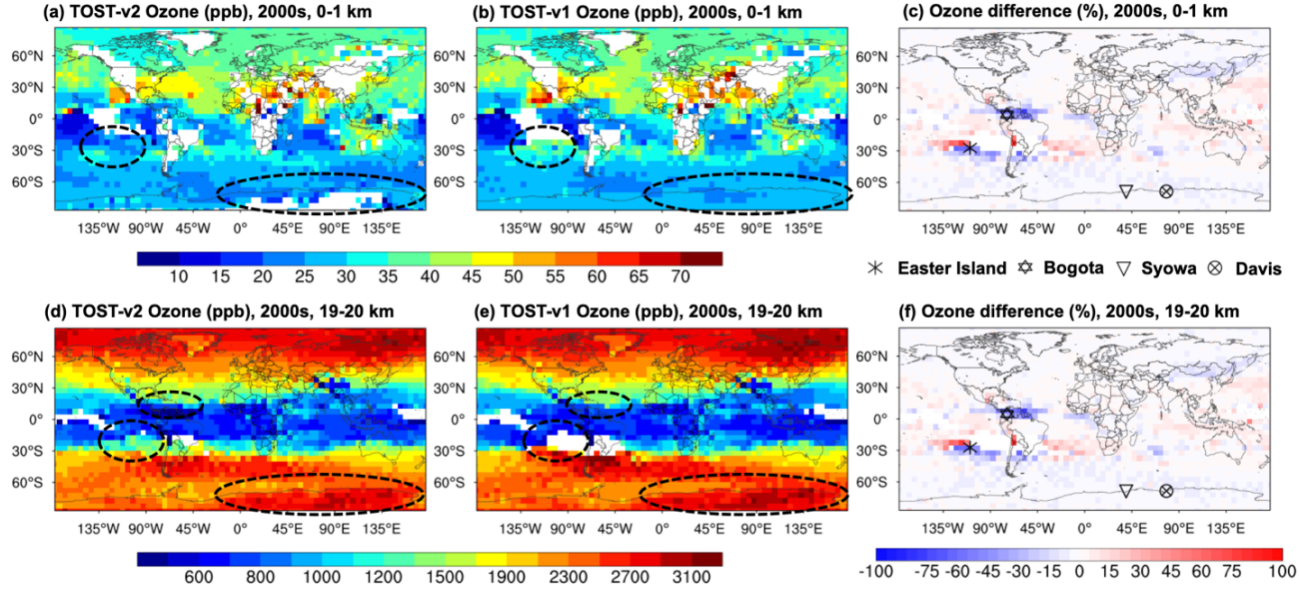

Figure 9. **(a, b)** The global distributions of ozone in TOST-v2 **(a)** and TOST-v1 **(b)** over 0–1 km in the 2000s. **(d, e)** The same as for **(a, b)**, but over 19–20 km. The dashed circles indicate regions with large differences between the two versions. **(c)** The global distributions of RD between TOST-v2 and TOST-v1 (RD = 100× (TOST-v2 − TOST-v1) / (0.5× TOST-v2 +0.5× TOST-v1); in %) over 0–1 km in the 2000s. **(f)** The same as for **(c)** but over 19–20 km. The markers indicate the positions of Davis, Easter Island, Bogotá and Syowa stations.

75th). TOST-v2 is also generated in a pressure altitude coordinate for users' convenience.

4 Global ozone spatial–temporal variations observed from TOST

4.1 Ozone spatial variations in the troposphere and stratosphere

As a 3-dimensional ozone dataset, TOST can depict both horizontal and vertical ozone distributions, as well as long-term ozone variation. Figure 10 shows distributions of decadal-mean TOST ozone at 3–4 and 19–20 km in four seasons of

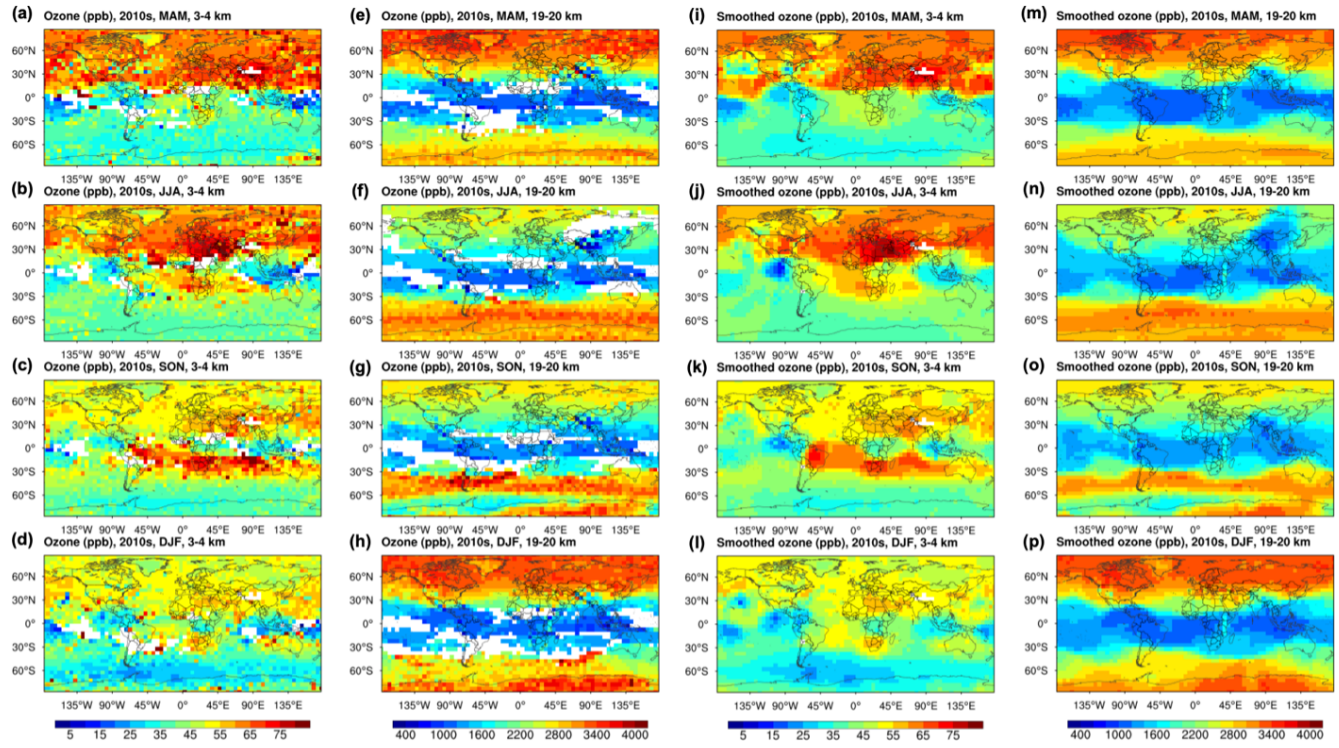

Figure 10. Global distribution of decadal-mean TOST ozone at 3–4 and 19–20 km in MAM (March–April–May), JJA (June–July–August), SON (September–October–November) and DJF (December–January–February) in the 2010s **(a–h)** and the corresponding smoothed TOST ozone **(i–p)**.

the 2000s. At 3–4 km in the troposphere, ozone concentrations are higher over the continent in the Northern Hemisphere, especially in MAM and DJF (> 50 ppb), reflecting the ozone production from the photochemical reactions of anthropogenic and natural emissions. In addition, the continental outflow from the southern USA (in MAM) and the biomass-burning-produced ozone in southern Africa (in JJA and SON) are well captured and in agreement with satellite observations (Fishman et al., 1990; Ebojie et al., 2016). At 19–20 km in the stratosphere (Fig. 10e–h), ozone concentrations are higher near the poles than in the tropics, due to the impact of the Brewer–Dobson circulation. The North Pole has higher ozone concentrations than the South Pole in DJF and MAM, and vice versa in JJA and SON, reflecting the seasonality of the Brewer–Dobson circulation. Also at 19–20 km, the ozone concentrations are lower over Asia in JJA (Fig. 10f) than in other seasons, reflecting the transport of ozone by the Asian summer monsoon from the tropics (Gettelman et al., 2004; Bian et al., 2020).

Although trajectory mapping fills in much of the global spatial domain, large gaps can still be found, particularly in the tropics, where ozone soundings are less dense. Since some applications require a default ozone value at all grid cells, a gap-filled and smoothed ozone dataset is also provided for the decadal-mean ozone in each month and the annual mean ozone, by fitting the maps at each level with a linear combination of spherical functions (Liu et al., 2013b). As shown in Fig. 10i–p, small-scale variations and extreme values are reduced in the smoothed ozone fields, while broad patterns of the ozone distribution are retained, making these smoothed maps valuable for qualitative visualization of the spatial, seasonal and decadal variations in ozone at different altitudes. They should, however, be used for any kind of quantitative analysis with great caution, as these data, where gaps exist in the unsmoothed TOST dataset, may be interpolated from the original measurement that is far in distance, and thus the degree to which they represent the true ozone value should be carefully examined. For example, erroneous conclusions have been inferred from the smoothed TOST-v1 over the tropics, with very limited observations before 1998, where the smoothed data were mostly interpolated from higher latitudes (Chipperfield et al., 2022). In addition, smoothing, as noted, filters small-scale variations and extreme values and retains ozone variations on large scales, which should be borne in mind when using the smoothed data. The smoothed dataset has not been quantitatively evaluated in any way.

Figure 11a–d show the latitude–altitude distribution of TOST ozone in each season averaged over 1970–2021. The steep changes in ozone concentration from < 100 to > 500 ppb in the vicinity of the tropopause (the black lines in Fig. 11a–d, calculated from the NCEP/NCAR reanaly-

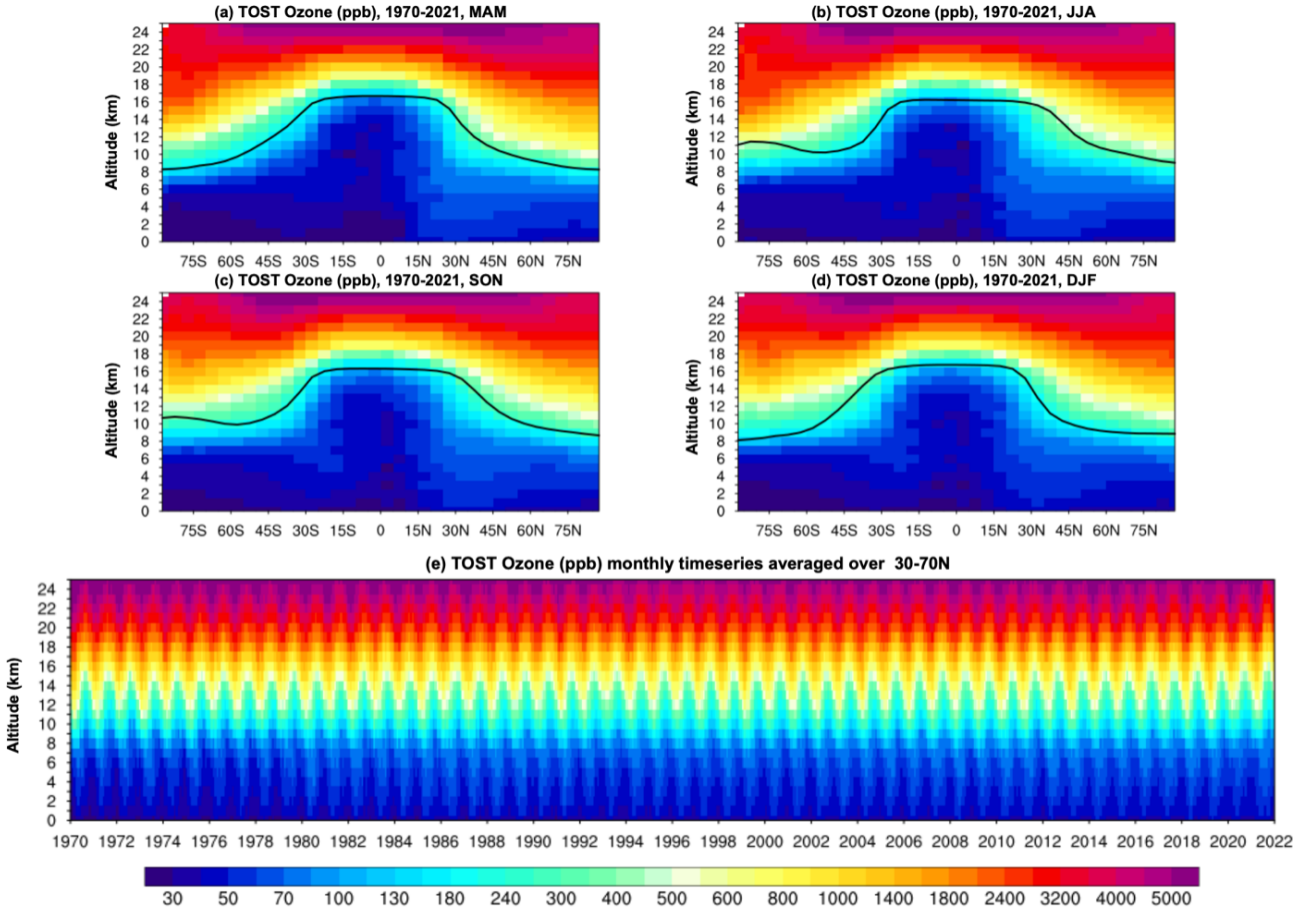

Figure 11. **(a–d)** The latitude–altitude distribution of TOST ozone averaged over 1970–2021 in each season. The solid black lines represent the mean tropopause height over 1970–2021 in each season. **(e)** Time series of the monthly mean TOST ozone over 30–70° N at each altitude level from 1970 to 2021.

sis) are well captured. Due to the Brewer–Dobson circulation, ozone concentrations above the tropopause increase with latitude from the tropics to the poles, which is also well reflected in the latitude–altitude distribution. TOST ozone concentrations around 12–13 km are higher in spring (600–800 ppb) than in the other seasons (< 500 ppb) over northern midlatitudes (45–60° N), which reflects the stronger Brewer–Dobson circulation in spring (Holton et al., 1995). Figure 11e shows the monthly mean TOST ozone time series from 1970 to 2021, averaged over 30–70° N at each level. Clear seasonal cycles are well captured every year.

4.2 Long-term trend in the lower stratospheric ozone

One of the advantages of TOST is its long-term coverage, which enables investigation of variations in ozone back to the 1970s. While analysis of long-term ozone trends in the troposphere with TOST is underway in separate projects, here we show an application of TOST data for studying lower-stratospheric ozone changes. Following the implementation of the Montreal Protocol and its amendments, recent studies have found an increase in upper stratospheric ozone since the late 1990s (Chipperfield et al., 2017; Szeląg et al., 2020; Dunn et al., 2023). However, the lower stratospheric ozone trend remains highly uncertain (Ball et al., 2020). Quantifying lower stratospheric ozone trends depends largely on the quality of the observational datasets (Li et al., 2023). While the trend is commonly analyzed with individual ozonesonde time series, it is challenging to assess how well individual long-term station changes represent regional or global variations. Combining data from sparse and widely separated ozonesonde sites involves implicit assumptions about their representativeness. With meteorological trajectory mapping, each original ozonesonde measurement is assigned a trajectory which describes its representativeness, and the TOST averages are therefore weighted according to the representativeness of each measurement. While this is subject to trajectory errors and the fact that coverage is incomplete (Table S3), unless trajectory errors are non-random, it should produce a better result than simple averaging of sonde station data by geographic region.

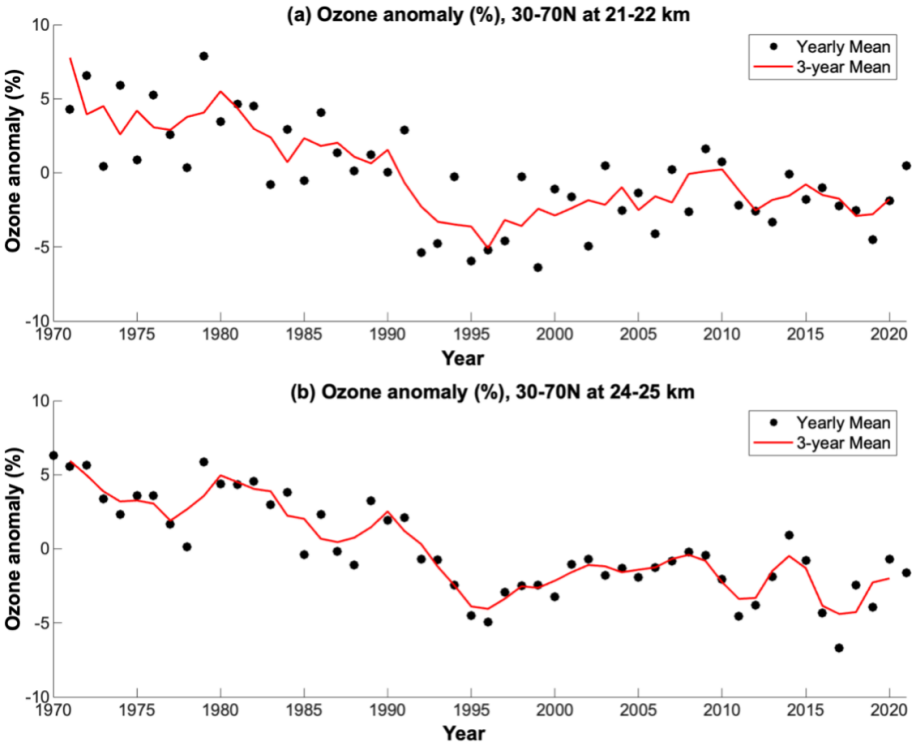

Figure 12. TOST time series of the annual mean ozone mixing ratios anomaly (in %) averaged over 30–70° N over 21–22 km altitude **(a)** and 24–25 km altitude **(b)**. The black dots represent the annual mean ozone concentrations from the area-weighted average of the grid cells over 30–70° N with ozone data throughout 1970–2021. The red line is the 3-year running mean.

Figure 12 shows the annual mean of ozone anomalies at 21–22 and 24–25 km from 1970 to 2021; the area-weighted averages were taken over grid cells from 30–70° N all with valid data throughout all years, i.e., ∼ 70 % of grid cells in the latitudinal zone. The 3-year running means are also shown with the time series. The ozone time series at both levels captures the clear ozone depletion before the early 1990s and the slow recovery in the latter part of the 1990s. In addition, these updated TOST time series show that stratospheric ozone has changed little since 2000. There are non-significant trends in the ozone concentrations at 21–22 km (0.5 ± 0.6 % per decade) and 24–25 km (-0.2 ± 0.9 % per decade) from 1998 to 2021, indicating little change of lower stratospheric ozone, despite the fact that 25 years has passed since peak stratospheric chlorine. Recent studies using merged satellite data suggested that the decrease in the lower stratospheric ozone is offsetting the increase in the upper stratosphere (Ball et al., 2018, 2019; Szeląg et al., 2020; Li et al., 2023), which is responsible for the flat trend in the total column ozone since the late 1990s. However, in the Northern Hemisphere midlatitudes, TOST indicates no significant trend in the lower stratospheric ozone after the late 1990s. The difference between the TOST and satellite-based data calls for further in-depth studies on the stratospheric ozone trend, especially in the lower stratosphere. Such observations of the variation in stratospheric ozone are essential to verifying the expected stratospheric ozone recovery under the Montreal Protocol and to understanding the feedbacks among dynamical, thermal and ozone variability.

5 Conclusions

An improved version of TOST has been constructed from 1970 to 2021 based on the updated ozonesonde profiles at 141 ozonesonde stations from WOUDC, SHADOZ, HEGIFTOM and NDACC (Table 1). The updated TOST was derived by combining the 4 d forward and backward trajectories from each ozonesonde profile, which were driven by the most state-of-the-art HYSPLIT model (v5.2) and NCEP reanalysis data (NNRP-1). Similar to TOST-v1, ozone concentrations in each season, in each year (1970–2021) and in each month of a decade (January to December from the 1970s to 2010s) are provided in 3-dimensional grids of $5° \times 5° \times 1$ km (latitude, longitude and altitude). For users' convenience, the corresponding spatially smoothed datasets are also provided for qualitative visualization, model initialization and other applications. TOST is provided in geometric coordinates from both sea level and ground level at 26 layers from the surface to the middle stratosphere; separate ozone climatology datasets are generated using ozonesonde profiles in both the troposphere and stratosphere, only in the troposphere, and only in the stratosphere. Statistics of standard

error and an independent number of samples are also provided. In TOST-v2, the corresponding datasets are also provided in a pressure altitude coordinate. In addition to the seasonal, annual or decadal monthly means, the corresponding datasets for ozone variations at three percentile levels (25, 50 and 75th) are also provided.

Comprehensive validation of TOST-v2 was conducted. At all the ozonesonde stations used, trajectory-derived ozone profiles without the input of the station itself were compared with the corresponding ozonesonde profiles at the stations. The overall comparison between the ozonesonde and trajectory-derived ozone shows good agreement in both the troposphere ($R = 0.56$–0.69, RD $= 2\,\%$–$4\,\%$) and stratosphere ($R = 0.97$, RD $= 0.5\,\%$) in each decade and in the mean of all decades (Fig. 2). The frequency distribution of RD at different altitudes shows interquartile ranges of RD between $-30\,\%$ and $30\,\%$, with the lowest interquartile ranges of RD ($-10\,\%$ to $10\,\%$) in the stratosphere and lower troposphere and no systematic bias except in the surface layer (Fig. 3). The vertical and seasonal variations of ozone profiles at individual stations are also well captured and quantified, with $R > 0.76$ and RD of $2\,\%$–$8\,\%$ (Fig. 4). Larger discrepancies are shown near the PBL and UTLS, especially for coastal stations where the trajectory-derived ozone may be biased by trajectories from the continent (Tarasick et al., 2010).

The comparison between TOST and satellite data, i.e., SAGE in the 1980s and 1990s, and MLS in the 2000s and 2010s, illustrates that TOST data have comparable accuracy with the satellite data in the stratosphere, while in the troposphere TOST is markedly superior (Fig. 5). In different latitude zones and decades, TOST performs comparably with SAGE and MLS data as well (Fig. S3 and Table S3). TOST-v2 was also directly compared to MOZAIC-IAGOS ozone profiles over the period 1994–2021 in the troposphere. Despite the systematic difference between MOZAIC-IAGOS and ozonesonde measurements, the two ozone datasets agree well in the monthly mean of 1994–2021 for the lower troposphere (RD $= 6\,\%$, Fig. 6).The uncertainties of TOST are largely dependent on the availability of ozonesonde data. Higher uncertainties are found before the 1990s, as global coverage is sparse in the tropics before the SHADOZ project. Higher uncertainties also appear at southern high latitudes and in the northern tropics (Fig. 8), likely because of greater ozone variability there, although biases between ozonesonde types may also contribute. TOST data at the PBL and UTLS have twice the RDs compared to other altitude levels; the former is due to more small-scale processes in the PBL, while the latter is related to the large ozone gradient and the dynamic variation of the tropopause. In addition, the smoothed dataset should be used for quantitative analysis with great caution, as it has not been quantitatively evaluated in any way.

Compared to the previous version of TOST (TOST-v1, Liu et al., 2013a, b), TOST-v2 is mainly improved in two aspects. Firstly, the record is extended to 2021, and data coverage is increased by as much as 15 %, as more ozone profiles and 43 additional ozonesonde stations are used in constructing the new version of TOST. Secondly, the spatial distribution of ozone has better agreement with ozonesonde measurements in both the troposphere and stratosphere over regions of Antarctica and the eastern Pacific, with RD decreased by $> 50\,\%$. Here we suggest future TOST improvement in three ways: applying more sophisticated meteorological reanalysis data to generate trajectories, using varying trajectory lengths based on the lifetime of ozone at different altitudes, and filling remaining gaps through reliable and effective gap-filling approaches. Moreover, including a tropopause referenced ozone climatology in the TOST dataset would help better comparisons with model data in the UTLS.

TOST can capture global ozone distributions in the troposphere and stratosphere (Figs. 10 and 11), showing horizontal and vertical variations, the continental outflow, and the gradient of ozone concentrations near the tropopause. TOST can also reflect the seasonal variations in ozone concentrations near the vicinity of the tropopause. Over the Northern Hemispheric midlatitudes, the time series of the updated TOST shows a stagnant recovery but an overall non-significant trend in lower stratospheric ozone after 1998 (Fig. 12), which is different from the decreasing trend reported in satellite-based data (Ball et al., 2018, 2019; Szeląg et al., 2020; Li et al., 2023). This calls for further exploration of stratospheric ozone trends, especially in the lower stratosphere.

It is anticipated that the TOST-v2 dataset can benefit future studies, owing to its long record, global coverage and high vertical resolution. We expect that it will be a useful dataset for trend studies, especially in the free troposphere, and also in the stratosphere, given the excellent long-term stability of the global ozonesonde network (Stauffer et al., 2022). We caution, however, that users should keep in mind the assumptions and limitations of the data product as described here.

Code and data availability. The ozonesonde data used in this study can be obtained from the WOUDC (https://doi.org/10.14287/10000001, WMO/GAW Ozone Monitoring Community et al., 2024), SHADOZ (https://doi.org/10.57721/SHADOZ-V06; SHADOZ, 2024) and HEGIFTOM (https://hegiftom.meteo.be/datasets/ozonesondes; TOAR-II HEGIFTOM Focus Working Group, 2024). The trajectory model HYSPLIT (version 5.2) is from the NOAA Air Resources Laboratory (http://www.arl.noaa.gov/ready.html; NOAA, 2024), driven by the NCEP/NCAR reanalysis data from the NOAA/OAR/ESRL PSD, Boulder, Colorado, USA, at https://www.ready.noaa.gov/data/archives/reanalysis/ (NCEP-NCAR, 2024). The aircraft data can be accessed from IAGOS network (https://www.iagos.org/; IAGOS, 2024). The two satellite data for comparison, the SAGE II (version 7.0) and the MLS (version 5.0), are obtained from https://doi.org/10.5067/ERBS/SAGEII/SOLAR_BINARY_L2-

V7.0 (NASA/LARC/SD/ASDC, 2012) and https://disc.gsfc.nasa.gov/datasets/ML2O3_005/summary?keywords=ML2O3_005 (Livesey et al., 2022), respectively. We are in the process of making the TOST available on the WOUDC website. TOST data currently are available at https://doi.org/10.5281/zenodo.13984482 (Zang et al., 2024).

Supplement. The supplement related to this article is available online at: https://doi.org/10.5194/acp-24-13889-2024-supplement.

Author contributions. JL and DT conceptualized and designed this study. ZZ performed data processing and analysis and composed the first draft. ZZ, JL and DT revised the manuscript with input from all the coauthors. All the coauthors contributed substantially to this study in making ozonesonde measurements; processing, calibrating and archiving the ozonesonde data; and providing constructive and valuable suggestions to and comments on the manuscript. All the coauthors approved the submission of this paper.

Competing interests. The contact author has declared that none of the authors has any competing interests.

Disclaimer. Publisher's note: Copernicus Publications remains neutral with regard to jurisdictional claims made in the text, published maps, institutional affiliations, or any other geographical representation in this paper. While Copernicus Publications makes every effort to include appropriate place names, the final responsibility lies with the authors.

Special issue statement. This article is part of the special issue "Tropospheric Ozone Assessment Report Phase II (TOAR-II) Community Special Issue (ACP/AMT/BG/GMD inter-journal SI)". It is not associated with a conference.

Acknowledgements. We thank many for their dedication to WOUDC, SHADOZ and HEGIFTOM, making ozonesonde data accessible. We also thank SAGE II and MLS team for their ozone data for comparison. We acknowledge the HYSPLIT team for the trajectory model. Zhou Zang and Jane Liu acknowledge the financial support from Natural Science and Engineering Council of Canada (grant no. RGPIN-2020-05163) and the Digital Research Alliance of Canada (https://alliancecan.ca, last access: 9 December 2024), and Jianchun Bian and Jinqiang Zhan acknowledge the financial support from the National Natural Science Foundation of China (grant no. 42293321). We are grateful to Michael Prather, Owen Cooper and an anonymous reviewer for their constructive comments and suggestions, which helped improve this paper.

Financial support. This research has been supported by the Natural Science and Engineering Council of Canada (grant no. RGPIN-2020-05163) and the National Natural Science Foundation of China (grant no. 42293321).

Review statement. This paper was edited by Simone Tilmes and reviewed by Michael Prather and one anonymous referee.

References

Ancellet, G. and Beekmann, M.: Ozone Monitoring and Measurements, in: Tropospheric Ozone Research: Tropospheric Ozone in the Regional and Sub-regional Context, Springer, 207–306, 1997.

Ancellet, G., Godin-Beekmann, S., Smit, H. G. J., Stauffer, R. M., Van Malderen, R., Bodichon, R., and Pazmiño, A.: Homogenization of the Observatoire de Haute Provence electrochemical concentration cell (ECC) ozonesonde data record: comparison with lidar and satellite observations, Atmos. Meas. Tech., 15, 3105–3120, https://doi.org/10.5194/amt-15-3105-2022, 2022.

Ball, W. T., Alsing, J., Mortlock, D. J., Staehelin, J., Haigh, J. D., Peter, T., Tummon, F., Stübi, R., Stenke, A., Anderson, J., Bourassa, A., Davis, S. M., Degenstein, D., Frith, S., Froidevaux, L., Roth, C., Sofieva, V., Wang, R., Wild, J., Yu, P., Ziemke, J. R., and Rozanov, E. V.: Evidence for a continuous decline in lower stratospheric ozone offsetting ozone layer recovery, Atmos. Chem. Phys., 18, 1379–1394, https://doi.org/10.5194/acp-18-1379-2018, 2018.

Ball, W. T., Alsing, J., Staehelin, J., Davis, S. M., Froidevaux, L., and Peter, T.: Stratospheric ozone trends for 1985–2018: sensitivity to recent large variability, Atmos. Chem. Phys., 19, 12731–12748, https://doi.org/10.5194/acp-19-12731-2019, 2019.

Ball, W. T., Chiodo, G., Abalos, M., Alsing, J., and Stenke, A.: Inconsistencies between chemistry–climate models and observed lower stratospheric ozone trends since 1998, Atmos. Chem. Phys., 20, 9737–9752, https://doi.org/10.5194/acp-20-9737-2020, 2020.

Bhartia, P. K.: OMI Algorithm Theoretical Basis Document Volume II, OMI Ozone, 2002.

Bian, J., Gettelman, A., Chen, H., and Pan, L. L.: Validation of satellite ozone profile retrievals using Beijing ozonesonde data, J. Geophys. Res.-Atmos., 112, D06305, https://doi.org/10.1029/2006JD007502, 2007.

Bian, J., Li, D., Bai, Z., Li, Q., Lyu, D., and Zhou, X.: Transport of Asian surface pollutants to the global stratosphere from the Tibetan Plateau region during the Asian summer monsoon, Natl. Sci. Rev., 7, 516–533, 2020.

Bodeker, G. E., Nitzbon, J., Tradowsky, J. S., Kremser, S., Schwertheim, A., and Lewis, J.: A global total column ozone climate data record, Earth Syst. Sci. Data, 13, 3885–3906, https://doi.org/10.5194/essd-13-3885-2021, 2021.

Bognar, K., Tegtmeier, S., Bourassa, A., Roth, C., Warnock, T., Zawada, D., and Degenstein, D.: Stratospheric ozone trends for 1984–2021 in the SAGE II–OSIRIS–SAGE II-I/ISS composite dataset, Atmos. Chem. Phys., 22, 9553–9569, https://doi.org/10.5194/acp-22-9553-2022, 2022.

Chen, X., Liu, Y., Lai, A., Han, S., Fan, Q., Wang, X., Ling, Z., Huang, F., and Fan, S.: Factors dominating 3-dimensional ozone

distribution during high tropospheric ozone period, Environ. Pollut., 232, 55–64, 2018.

Chipperfield, M. P., Bekki, S., Dhomse, S., Harris, N. R., Hassler, B., Hossaini, R., Steinbrecht, W., Thiéblemont, R., and Weber, M.: Detecting recovery of the stratospheric ozone layer, Nature, 549, 211–218, 2017.

Chipperfield, M. P., Chrysanthou, A., Damadeo, R., Dameris, M., Dhomse, S. S., Fioletov, V., Frith, S. M., Godin-Beekmann, S., Hassler, B., and Liu, J.: Comment on "Observation of large and all-season ozone losses over the tropics" [AIP Adv. 12, 075006 (2022)], AIP Adv., 12, 129102, https://doi.org/10.1063/5.0121723, 2022.

Chouza, F., Leblanc, T., Brewer, M., and Wang, P.: Upgrade and automation of the JPL Table Mountain Facility tropospheric ozone lidar (TMTOL) for near-ground ozone profiling and satellite validation, Atmos. Meas. Tech., 12, 569–583, https://doi.org/10.5194/amt-12-569-2019, 2019.

Colombi, N., Miyazaki, K., Bowman, K. W., Neu, J. L., and Jacob, D. J.: A new methodology for inferring surface ozone from multispectral satellite measurements, Environ. Res. Lett., 16, 105005, https://doi.org/10.1088/1748-9326/ac243d, 2021.

Cunnold, D., Wang, H., Chu, W., and Froidevaux, L.: Comparisons between Stratospheric Aerosol and Gas Experiment II and microwave limb sounder ozone measurements and aliasing of SAGE II ozone trends in the lower stratosphere, J. Geophys. Res.-Atmos., 101, 10061–10075, 1996.

Draxler, R. R. and Hess, G.: An overview of the HYSPLIT_4 modelling system for trajectories, Aust. Meteorol. Mag., 47, 295–308, 1998.

Dunn, R. J., Miller, J. B., Willett, K. M., Gobron, N., Ades, M., Adler, R., Alexe, M., Allan, R. P., Anderson, J., and Anneville, O.: Global climate, B. Am. Meteor. Soc., 104, S11–S145, 2023.

Ebojie, F., Burrows, J. P., Gebhardt, C., Ladstätter-Weißenmayer, A., von Savigny, C., Rozanov, A., Weber, M., and Bovensmann, H.: Global tropospheric ozone variations from 2003 to 2011 as seen by SCIAMACHY, Atmos. Chem. Phys., 16, 417–436, https://doi.org/10.5194/acp-16-417-2016, 2016.

Engström, A. and Magnusson, L.: Estimating trajectory uncertainties due to flow dependent errors in the atmospheric analysis, Atmos. Chem. Phys., 9, 8857–8867, https://doi.org/10.5194/acp-9-8857-2009, 2009.

Eyring, V., Cionni, I., Bodeker, G. E., Charlton-Perez, A. J., Kinnison, D. E., Scinocca, J. F., Waugh, D. W., Akiyoshi, H., Bekki, S., Chipperfield, M. P., Dameris, M., Dhomse, S., Frith, S. M., Garny, H., Gettelman, A., Kubin, A., Langematz, U., Mancini, E., Marchand, M., Nakamura, T., Oman, L. D., Pawson, S., Pitari, G., Plummer, D. A., Rozanov, E., Shepherd, T. G., Shibata, K., Tian, W., Braesicke, P., Hardiman, S. C., Lamarque, J. F., Morgenstern, O., Pyle, J. A., Smale, D., and Yamashita, Y.: Multi-model assessment of stratospheric ozone return dates and ozone recovery in CCMVal-2 models, Atmos. Chem. Phys., 10, 9451–9472, https://doi.org/10.5194/acp-10-9451-2010, 2010.

Fioletov, V., Tarasick, D., and Petropavlovskikh, I.: Estimating ozone variability and instrument uncertainties from SBUV (/2), ozonesonde, Umkehr, and SAGE II measurements: Short-term variations, J. Geophys. Res.-Atmos., 111, D02305, https://doi.org/10.1029/2005JD006340, 2006.

Fishman, J., Watson, C. E., Larsen, J. C., and Logan, J. A.: Distribution of tropospheric ozone determined from satellite data, J. Geophys. Res.-Atmos., 95, 3599–3617, 1990.

Fleming, Z. L., Doherty, R. M., Von Schneidemesser, E., Malley, C. S., Cooper, O. R., Pinto, J. P., Colette, A., Xu, X., Simpson, D., and Schultz, M. G.: Tropospheric Ozone Assessment Report: Present-day ozone distribution and trends relevant to human health, Elem. Sci. Anth., 6, 12, https://doi.org/10.1525/elementa.273, 2018.

Forster, P., Storelvmo, T., Armour, K., Collins, W., Dufresne, J.-L., Frame, D., Lunt, D. J., Mauritsen, T., Palmer, M. D., Watanabe, M., Wild, M., and Zhang, H.: The Earth's Energy Budget, Climate Feedbacks, and Climate Sensitivity, in: Climate Change 2021: The Physical Science Basis, Contribution of Working Group I to the Sixth Assessment Report of the Intergovernmental Panel on Climate Change, edited by: Masson-Delmotte, V., Zhai, P., Pirani, A., Connors, S. L., Péan, C., Berger, S., Caud, N., Chen, Y., Goldfarb, L., Gomis, M. I., Huang, M., Leitzell, K., Lonnoy, E., Matthews, J. B. R., Maycock, T. K., Waterfield, T., Yelekçi, O., Yu, R., and Zhou, B., Cambridge University Press, Cambridge, United Kingdom and New York, NY, USA, 923–1054, https://doi.org/10.1017/9781009157896.009, 2021.

Gaudel, A., Cooper, O. R., Ancellet, G., Barret, B., Boynard, A., Burrows, J. P., Clerbaux, C., Coheur, P.-F., Cuesta, J., and Cuevas, E.: Tropospheric Ozone Assessment Report: Present-day distribution and trends of tropospheric ozone relevant to climate and global atmospheric chemistry model evaluation, Elementa: Science of the Anthropocene, 6, 39, https://doi.org/10.1525/elementa.291, 2018.

Gettelman, A., Kinnison, D. E., Dunkerton, T. J., and Brasseur, G. P.: Impact of monsoon circulations on the upper troposphere and lower stratosphere, J. Geophys. Res.-Atmos., 109, D22101, https://doi.org/10.1029/2004JD004878, 2004.

Greenslade, J. W., Alexander, S. P., Schofield, R., Fisher, J. A., and Klekociuk, A. K.: Stratospheric ozone intrusion events and their impacts on tropospheric ozone in the Southern Hemisphere, Atmos. Chem. Phys., 17, 10269–10290, https://doi.org/10.5194/acp-17-10269-2017, 2017.

Griffiths, P. T., Murray, L. T., Zeng, G., Shin, Y. M., Abraham, N. L., Archibald, A. T., Deushi, M., Emmons, L. K., Galbally, I. E., Hassler, B., Horowitz, L. W., Keeble, J., Liu, J., Moeini, O., Naik, V., O'Connor, F. M., Oshima, N., Tarasick, D., Tilmes, S., Turnock, S. T., Wild, O., Young, P. J., and Zanis, P.: Tropospheric ozone in CMIP6 simulations, Atmos. Chem. Phys., 21, 4187–4218, https://doi.org/10.5194/acp-21-4187-2021, 2021.

Gulev, S. K., Thorne, P. W., Ahn, J., Dentener, F. J., Domingues, C. M., Gerland, S., Gong, D. S., Kaufman, S., Nnamchi, H. C., Quaas, J., Rivera, J. A., Sathyendranath, S., Smith, S. L., Trewin, B., von Shuckmann, K., and Vose, R. S.: Changing State of the Climate System, in: Climate Change 2021: The Physical Science Basis. Contribution of Working Group I to the Sixth Assessment Report of the Intergovernmental Panel on Climate Change, edited by: Masson-Delmotte, V., Zhai, P., Pirani, A., Connors, S. L., Péan, C., Berger, S., Caud, N., Chen, Y., Goldfarb, L., Gomis, M. I., Huang, M., Leitzell, K., Lonnoy, E., Matthews, J. B. R., Maycock, T.K., Waterfield, T., Yelekçi, O., Yu, R., and Zhou, B., Cambridge University Press, Cambridge, United Kingdom and New York, NY, USA, 287–422, https://doi.org/10.1017/9781009157896.004, 2021.

Han, H., Liu, J., Yuan, H., Wang, T., Zhuang, B., and Zhang, X.: Foreign influences on tropospheric ozone over East Asia through global atmospheric transport, Atmos. Chem. Phys., 19, 12495–12514, https://doi.org/10.5194/acp-19-12495-2019, 2019.

Harmens, H., Hayes, F., Mills, G., Sharps, K., Osborne, S., and Pleijel, H.: Wheat yield responses to stomatal uptake of ozone: Peak vs rising background ozone conditions, Atmos. Environ., 173, 1–5, 2018.

Hassler, B., Bodeker, G. E., and Dameris, M.: Technical Note: A new global database of trace gases and aerosols from multiple sources of high vertical resolution measurements, Atmos. Chem. Phys., 8, 5403–5421, https://doi.org/10.5194/acp-8-5403-2008, 2008.

Hassler, B., Kremser, S., Bodeker, G. E., Lewis, J., Nesbit, K., Davis, S. M., Chipperfield, M. P., Dhomse, S. S., and Dameris, M.: An updated version of a gap-free monthly mean zonal mean ozone database, Earth Syst. Sci. Data, 10, 1473–1490, https://doi.org/10.5194/essd-10-1473-2018, 2018.

Holton, J. R., Haynes, P. H., McIntyre, M. E., Douglass, A. R., Rood, R. B., and Pfister, L.: Stratosphere-troposphere exchange, Rev. Geophys., 33, 403–439, 1995.

Huijnen, V., Miyazaki, K., Flemming, J., Inness, A., Sekiya, T., and Schultz, M. G.: An intercomparison of tropospheric ozone reanalysis products from CAMS, CAMS interim, TCR-1, and TCR-2, Geosci. Model Dev., 13, 1513–1544, https://doi.org/10.5194/gmd-13-1513-2020, 2020.

IAGOS: IAGOS-CORE, IAGOS-MOZAIC, IAGOS-CARIBIC, https://iagos.aeris-data.fr/download/ (last access: 25 October, 2024), 2024.

Kalney, E., Kanamitsu, M., Kistler, R., Collins, W., Deaven, D., Gandin, L., Iredell, M., Saha, S., White, G., Woollen, J., Zhu, Y., Chelliah, M., Ebisuzaki, W., Higgins, W., Janowiak, J., Mo, K. C., Ropelewski, C., Wang, J., Leetmaa, A., Reynolds, R., Jenne, R., and Joseph, D.: The NCEP/NCAR 40-Year Reanalysis Project, B.e Am. Meteor. Soc., 77, 437–472, 1996.

Kent, G., Winker, D., Osborn, M., and Skeens, K.: A model for the separation of cloud and aerosol in SAGE II occultation data, J. Geophys. Res.-Atmos., 98, 20725–20735, 1993.

Keppens, A., Lambert, J.-C., Granville, J., Miles, G., Siddans, R., van Peet, J. C. A., van der A, R. J., Hubert, D., Verhoelst, T., Delcloo, A., Godin-Beekmann, S., Kivi, R., Stübi, R., and Zehner, C.: Round-robin evaluation of nadir ozone profile retrievals: methodology and application to MetOp-A GOME-2, Atmos. Meas. Tech., 8, 2093–2120, https://doi.org/10.5194/amt-8-2093-2015, 2015.

Kremser, S., Thomason, L. W., and Bird, L. J.: Simplified SAGE II ozone data usage rules, Earth Syst. Sci. Data, 12, 1419–1435, https://doi.org/10.5194/essd-12-1419-2020, 2020.

Li, Y., Dhomse, S. S., Chipperfield, M. P., Feng, W., Bian, J., Xia, Y., and Guo, D.: Quantifying stratospheric ozone trends over 1984–2020: a comparison of ordinary and regularized multivariate regression models, Atmos. Chem. Phys., 23, 13029–13047, https://doi.org/10.5194/acp-23-13029-2023, 2023.

Liu, G., Tarasick, D. W., Fioletov, V. E., Sioris, C. E., and Rochon, Y. J.: Ozone correlation lengths and measurement uncertainties from analysis of historical ozonesonde data in North America and Europe, J. Geophys. Res.-Atmos., 114, D04112, https://doi.org/10.1029/2008JD010576, 2009.

Liu, G., Liu, J., Tarasick, D. W., Fioletov, V. E., Jin, J. J., Moeini, O., Liu, X., Sioris, C. E., and Osman, M.: A global tropospheric ozone climatology from trajectory-mapped ozone soundings, Atmos. Chem. Phys., 13, 10659–10675, https://doi.org/10.5194/acp-13-10659-2013, 2013a.

Liu, J., Tarasick, D. W., Fioletov, V. E., McLinden, C., Zhao, T., Gong, S., Sioris, C., Jin, J. J., Liu, G., and Moeini, O.: A global ozone climatology from ozone soundings via trajectory mapping: a stratospheric perspective, Atmos. Chem. Phys., 13, 11441–11464, https://doi.org/10.5194/acp-13-11441-2013, 2013b.

Liu, X., Bhartia, P. K., Chance, K., Spurr, R. J. D., and Kurosu, T. P.: Ozone profile retrievals from the Ozone Monitoring Instrument, Atmos. Chem. Phys., 10, 2521–2537, https://doi.org/10.5194/acp-10-2521-2010, 2010.

Livesey, N., Read, W., Wagner, P., Froidevaux, L., Santee, M., Schwartz, M., Lambert, A., Millán Valle, L., Pumphrey, H., and Manney, G.: Earth Observing System (EOS) Aura Microwave Limb Sounder (MLS) version 5.0 x level 2 and 3 data quality and description document Version 5.0–1.1 a (Tech. Rep.), Jet Propulsion Laboratory, California Institute of Technology, https://mls.jpl.nasa.gov/data/v5-0_data_quality_document.pdf (last access: 25 October 2024), 2022.

McDermid, I. S., Beyerle, G., Haner, D. A., and Leblanc, T.: Redesign and improved performance of the tropospheric ozone lidar at the Jet Propulsion Laboratory Table Mountain Facility, Appl. Opt., 41, 7550–7555, https://doi.org/10.1364/AO.41.007550, 2002.

McPeters, R. D. and Labow, G. J.: Climatology 2011: An MLS and sonde derived ozone climatology for satellite retrieval algorithms, J. Geophys. Res.-Atmos., 117, D10303, https://doi.org/10.1029/2011JD017006, 2012.

McPeters, R. D., Labow, G. J., and Logan, J. A.: Ozone climatological profiles for satellite retrieval algorithms, J. Geophys. Res.-Atmos., 112, D05308, https://doi.org/10.1029/2005JD006823, 2007.

Millán, L. F., Manney, G. L., Boenisch, H., Hegglin, M. I., Hoor, P., Kunkel, D., Leblanc, T., Petropavlovskikh, I., Walker, K., Wargan, K., and Zahn, A.: Multi-parameter dynamical diagnostics for upper tropospheric and lower stratospheric studies, Atmos. Meas. Tech., 16, 2957–2988, https://doi.org/10.5194/amt-16-2957-2023, 2023.

Mills, G., Pleijel, H., Malley, C. S., Sinha, B., Cooper, O. R., Schultz, M. G., Neufeld, H. S., Simpson, D., Sharps, K., and Feng, Z.: Tropospheric Ozone Assessment Report: Present-day tropospheric ozone distribution and trends relevant to vegetation, Elem. Sci. Anth., 6, 47, https://doi.org/10.1525/elementa.302, 2018.

Miyazaki, K., Bowman, K. W., Yumimoto, K., Walker, T., and Sudo, K.: Evaluation of a multi-model, multi-constituent assimilation framework for tropospheric chemical reanalysis, Atmos. Chem. Phys., 20, 931–967, https://doi.org/10.5194/acp-20-931-2020, 2020a.

Miyazaki, K., Bowman, K., Sekiya, T., Eskes, H., Boersma, F., Worden, H., Livesey, N., Payne, V. H., Sudo, K., Kanaya, Y., Takigawa, M., and Ogochi, K.: Updated tropospheric chemistry reanalysis and emission estimates, TCR-2, for 2005–2018, Earth Syst. Sci. Data, 12, 2223–2259, https://doi.org/10.5194/essd-12-2223-2020, 2020b.

Moeini, O., Tarasick, D. W., McElroy, C. T., Liu, J., Osman, M. K., Thompson, A. M., Parrington, M., Palmer, P. I., Johnson, B., and Oltmans, S. J.: Estimating wildfire-generated ozone over North America using ozonesonde profiles and a differential back trajectory technique, Atmos. Environ.: X, 7, 100078, https://doi.org/10.1016/j.aeaoa.2020.100078, 2020.

NASA/LARC/SD/ASDC: Stratospheric Aerosol and Gas Experiment (SAGE) II Version 7.0 Aerosol, O_3, NO_2 and H_2O Profiles in binary format, Atmospheric Science Data Center [data set], https://doi.org/10.5067/ERBS/SAGEII/SOLAR_BINARY_L2-V7.0, 2013.

NCEP–NCAR: Reanalisys 1, NOAA Physical Sciences Laboratory, https://downloads.psl.noaa.gov/Datasets/ncep.reanalysis/pressure/ (last access: 25 October 2024), 2024.

Nédélec, P., Blot, R., Boulanger, D., Athier, G., Cousin, J.-M., Gautron, B., Petzold, A., Volz-Thomas, A., and Thouret, V.: Instrumentation on commercial aircraft for monitoring the atmospheric composition on a global scale: the IAGOS system, technical overview of ozone and carbon monoxide measurements, Tellus B, 67, 27791, https://doi.org/10.3402/tellusb.v67.27791, 2015.

NOAA: HYSPLIT model, NOAA Air Resources Laboratory, NOAA, https://www.ready.noaa.gov/HYSPLIT.php (last access: 25 October 2024), 2024.

Nowack, P. J., Luke Abraham, N., Maycock, A. C., Braesicke, P., Gregory, J. M., Joshi, M. M., Osprey, A., and Pyle, J. A.: A large ozone-circulation feedback and its implications for global warming assessments, Nat. Clim. Change, 5, 41–45, 2015.

Petetin, H., Sauvage, B., Smit, H. G. J., Gheusi, F., Lohou, F., Blot, R., Clark, H., Athier, G., Boulanger, D., Cousin, J.-M., Nedelec, P., Neis, P., Rohs, S., and Thouret, V.: A climatological view of the vertical stratification of RH, O_3 and CO within the PBL and at the interface with free troposphere as seen by IAGOS aircraft and ozonesondes at northern mid-latitudes over 1994–2016, Atmos. Chem. Phys., 18, 9561–9581, https://doi.org/10.5194/acp-18-9561-2018, 2018.

Petzold, A., Thouret, V., Gerbig, C., Zahn, A., Brenninkmeijer, C. A., Gallagher, M., Hermann, M., Pontaud, M., Ziereis, H., and Boulanger, D.: Global-scale atmosphere monitoring by in-service aircraft–current achievements and future prospects of the European Research Infrastructure IAGOS, Tellus B, 67, 28452, https://doi.org/10.3402/tellusb.v67.28452, 2015.

Polvani, L. M., Wang, L., Aquila, V., and Waugh, D. W.: The impact of ozone-depleting substances on tropical upwelling, as revealed by the absence of lower-stratospheric cooling since the late 1990s, J. Climate, 30, 2523–2534, 2017.

Prather, M. J. and Zhu, X.: Lifetimes and timescales of tropospheric ozone: Global metrics for climate change, human health, and crop/ecosystem research, Elementa: Science of the Anthropocene, 12, 1, https://doi.org/10.1525/elementa.2023.00112,, 2024.

Prather, M. J., Guo, H., and Zhu, X.: Deconstruction of tropospheric chemical reactivity using aircraft measurements: the Atmospheric Tomography Mission (ATom) data, Earth Syst. Sci. Data, 15, 3299–3349, https://doi.org/10.5194/essd-15-3299-2023, 2023.

Rahpoe, N., Weber, M., Rozanov, A. V., Weigel, K., Bovensmann, H., Burrows, J. P., Laeng, A., Stiller, G., von Clarmann, T., Kyrölä, E., Sofieva, V. F., Tamminen, J., Walker, K., Degenstein, D., Bourassa, A. E., Hargreaves, R., Bernath, P., Urban, J., and Murtagh, D. P.: Relative drifts and biases between six ozone limb satellite measurements from the last decade, Atmos. Meas. Tech., 8, 4369–4381, https://doi.org/10.5194/amt-8-4369-2015, 2015.

SHADOZ: SHADOZ ozone profiles, NASA/Goddard Space Flight Center [data set], https://doi.org/10.57721/SHADOZ-V06, 2024.

Sicard, M., Granados-Muñoz, M. J., Alados-Arboledas, L., Barragán, R., Bedoya-Velásquez, A. E., Benavent-Oltra, J. A., Bortoli, D., Comerón, A., Córdoba-Jabonero, C., and Costa, M. J.: Ground/space, passive/active remote sensing observations coupled with particle dispersion modelling to understand the inter-continental transport of wildfire smoke plumes, Remote Sens. Environ., 232, 111294, https://doi.org/10.1016/j.rse.2019.111294, 2019.

Smit, H. and Thompson, A. M.: Ozonesonde Measurement Principles and Best Operational Practices ASOPOS 2.0 (Assessment of Standard Operating Procedures for Ozonesondes), GAW Report No. 268, https://library.wmo.int/idurl/4/57720 (last access: 3 December 2024), 2021.

Smit, H. G. and Kley, D.: JOSIE: The 1996 WMO International intercomparison of ozonesondes under quasi flight conditions in the environmental simulation chamber at Jülich, Proceedings of the XVIII Quadrennial Ozone Symposium, 971–974, Geneva, Switzerland, 1998.

Staufer, J., Staehelin, J., Stübi, R., Peter, T., Tummon, F., and Thouret, V.: Trajectory matching of ozonesondes and MOZAIC measurements in the UTLS – Part 1: Method description and application at Payerne, Switzerland, Atmos. Meas. Tech., 6, 3393–3406, https://doi.org/10.5194/amt-6-3393-2013, 2013.

Staufer, J., Staehelin, J., Stübi, R., Peter, T., Tummon, F., and Thouret, V.: Trajectory matching of ozonesondes and MOZAIC measurements in the UTLS – Part 2: Application to the global ozonesonde network, Atmos. Meas. Tech., 7, 241–266, https://doi.org/10.5194/amt-7-241-2014, 2014.

Stauffer, R. M., Thompson, A. M., Kollonige, D. E., Witte, J. C., Tarasick, D. W., Davies, J., Vömel, H., Morris, G. A., Van Malderen, R., and Johnson, B. J.: A post-2013 dropoff in total ozone at a third of global ozonesonde stations: Electrochemical concentration cell instrument artifacts? Geophys. Res. Lett., 47, e2019GL086791, https://doi.org/10.1029/2019GL086791, 2020.

Stauffer, R. M., Thompson, A. M., Kollonige, D. E., Tarasick, D. W., Van Malderen, R., Smit, H. G., Vömel, H., Morris, G. A., Johnson, B. J., and Cullis, P. D.: An examination of the recent stability of ozonesonde global network data, Earth Space Sci., 9, e2022EA002459, https://doi.org/10.1029/2022EA002459, 2022.

Stein, A., Draxler, R. R., Rolph, G. D., Stunder, B. J., Cohen, M., and Ngan, F.: NOAA's HYSPLIT atmospheric transport and dispersion modeling system, B. Am. Meteor. Soc., 96, 2059–2077, 2015.

Steinbrecht, W., Froidevaux, L., Fuller, R., Wang, R., Anderson, J., Roth, C., Bourassa, A., Degenstein, D., Damadeo, R., Zawodny, J., Frith, S., McPeters, R., Bhartia, P., Wild, J., Long, C., Davis, S., Rosenlof, K., Sofieva, V., Walker, K., Rahpoe, N., Rozanov, A., Weber, M., Laeng, A., von Clarmann, T., Stiller, G., Kramarova, N., Godin-Beekmann, S., Leblanc, T., Querel, R., Swart, D., Boyd, I., Hocke, K., Kämpfer, N., Maillard Barras, E., Moreira, L., Nedoluha, G., Vigouroux, C., Blumenstock, T., Schneider, M., García, O., Jones, N., Mahieu, E., Smale, D., Kotkamp, M., Robinson, J., Petropavlovskikh, I., Harris, N., Hassler, B.,

Hubert, D., and Tummon, F.: An update on ozone profile trends for the period 2000 to 2016, Atmos. Chem. Phys., 17, 10675–10690, https://doi.org/10.5194/acp-17-10675-2017, 2017.

Sterling, C. W., Johnson, B. J., Oltmans, S. J., Smit, H. G. J., Jordan, A. F., Cullis, P. D., Hall, E. G., Thompson, A. M., and Witte, J. C.: Homogenizing and estimating the uncertainty in NOAA's long-term vertical ozone profile records measured with the electrochemical concentration cell ozonesonde, Atmos. Meas. Tech., 11, 3661–3687, https://doi.org/10.5194/amt-11-3661-2018, 2018.

Stohl, A.: Computation, accuracy and applications of trajectories – A review and bibliography, Atmos. Environ., 32, 947–966, 1998.

Stohl, A. and Seibert, P.: Accuracy of trajectories as determined from the conservation of meteorological tracers, Q. J. Roy. Meteor. Soc., 124, 1465–1484, 1998.

Stohl, A., James, P., Forster, C., Spichtinger, N., Marenco, A., Thouret, V., and Smit, H. G.: An extension of Measurement of Ozone and Water Vapour by Airbus In-service Aircraft (MOZAIC) ozone climatologies using trajectory statistics, J. Geophys. Res.-Atmos., 106, 27757–27768, 2001.

Stohl, A., Eckhardt, S., Forster, C., James, P., Spichtinger, N., and Seibert, P.: A replacement for simple back trajectory calculations in the interpretation of atmospheric trace substance measurements, Atmos. Environ., 36, 4635–4648, 2002.

Szeląg, M. E., Sofieva, V. F., Degenstein, D., Roth, C., Davis, S., and Froidevaux, L.: Seasonal stratospheric ozone trends over 2000–2018 derived from several merged data sets, Atmos. Chem. Phys., 20, 7035–7047, https://doi.org/10.5194/acp-20-7035-2020, 2020.

Szopa, S., Naik, V., Adhikary, B., Artaxo, P., Berntsen, T., Collins, W. D., Fuzzi, S., Gallardo, L., Kiendler-Scharr, A., Klimont, Z., Liao, H., Unger, N., and Zanis, P.: Short-lived Climate Forcers, Climate Change 2021: The Physical Science Basis, Contribution of Working Group I to the Sixth Assessment Report of the Intergovernmental Panel on Climate Change, Masson-Delmotte, V., Zhai, P., Pirani, A., Connors, S. L., Péan, C., Berger, S., Caud, N., Chen, Y., Goldfarb, L., Gomis, M. I., Huang, M., Leitzell, K., Lonnoy, E., Matthews, J. B. R., Maycock, T.K., Waterfield, T., Yelekçi, O., Yu, R., and Zhou, B., Cambridge University Press, Cambridge, United Kingdom and New York, NY, USA, 817–922, https://doi.org/10.1017/9781009157896.008, 2021.

Tanimoto, H., Zbinden, R. M., Thouret, V., and Nédélec, P.: Consistency of tropospheric ozone observations made by different platforms and techniques in the global databases, Tellus B, 67, 27073, https://doi.org/10.3402/tellusb.v67.27073, 2015.

Tarasick, D., Jin, J., Fioletov, V., Liu, G., Thompson, A., Oltmans, S., Liu, J., Sioris, C., Liu, X., and Cooper, O.: High-resolution tropospheric ozone fields for INTEX and ARCTAS from IONS ozonesondes, J. Geophys. Res.-Atmos., 115, D20301, https://doi.org/10.1029/2009JD012918, 2010.

Tarasick, D., Carey-Smith, T., Hocking, W., Moeini, O., He, H., Liu, J., Osman, M., Thompson, A., Johnson, B., and Oltmans, S.: Quantifying stratosphere-troposphere transport of ozone using balloon-borne ozonesondes, radar windprofilers and trajectory models, Atmos. Environ., 198, 496–509, 2019.

Tarasick, D., Stauffer, R. M., Smit, H. G., Thompson, A. M., Davies, J., Van Malderen, R., Johnson, B., and Vömel, H.: Improving data quality in long-term Canadian ozone sounding records, XXVIII General Assembly of the International Union of Geodesy and Geophysics (IUGG), Berlin, https://doi.org/10.57757/IUGG23-4503, 2023.

Tarasick, D. W., Davies, J., Smit, H. G. J., and Oltmans, S. J.: A re-evaluated Canadian ozonesonde record: measurements of the vertical distribution of ozone over Canada from 1966 to 2013, Atmos. Meas. Tech., 9, 195–214, https://doi.org/10.5194/amt-9-195-2016, 2016.

Tarasick, D. W., Galbally, I., Cooper, O. R., Schultz, M. G., Ancellet, G., LeBlanc, T., Wallington, T. J., Ziemke, J., Liu, X., Steinbacher, M., Stähelin, J., Vigouroux, C., Hannigan, J., García, O., Foret, G., Zanis, P. Weatherhead, E., Petropavlovskikh, I., Worden, H., Neu, J. L., Osman, M., Liu, J., Lin, M., Granados-Muñoz, M., Thompson, A. M., Oltmans, S. J., Cuesta, J., Dufour, G., Thouret, V., Hassler, B., Thompson, A. M., and Trickl, T.: TOAR- Observations: Tropospheric ozone from 1877 to 2016, observed levels, trends and uncertainties, Elementa: Science of the Anthropocene, 7, 39, https://doi.org/10.1525/elementa.376, 2019.

Tarasick, D. W., Smit, H. G. J., Thompson, A. M., Morris, G. A., Witte, J. C., Davies, J., Nakano, T., van Malderen, R., Stauffer, R. M., Deshler, T., Johnson, B. J., Stübi, R., Oltmans, S. J., and Vömel, H.: Improving ECC ozonesonde data quality: Assessment of current methods and outstanding issues, Earth Space Sci., 8, e2019EA000914, https://doi.org/10.1029/2019EA000914, 2021.

Terao, Y., Logan, J. A., Douglass, A. R., and Stolarski, R. S.: Contribution of stratospheric ozone to the interannual variability of tropospheric ozone in the northern extratropics, J. Geophys. Res.-Atmos., 113, D18309, https://doi.org/10.1029/2008JD009854, 2008.

TOAR-II HEGIFTOM Focus Working Group: Ozonesondes, https://hegiftom.meteo.be/datasets (last access: 25 October 2024), 2024.

Thompson, A. M., Witte, J. C., Sterling, C., Jordan, A., Johnson, B. J., Oltmans, S. J., Fujiwara, M., Vömel, H., Allaart, M., and Piters, A.: First reprocessing of Southern Hemisphere Additional Ozonesondes (SHADOZ) ozone profiles (1998–2016): 2. Comparisons with satellites and ground-based instruments, J. Geophys. Res.-Atmos., 122, 13000–13025, 2017.

Thouret, V., Marenco, A., Logan, J. A., Nédélec, P., and Grouhel, C.: Comparisons of ozone measurements from the MOZAIC airborne program and the ozone sounding network at eight locations, J. Geophys. Res.-Atmos., 103, 25695–25720, 1998.

Tilmes, S., Lamarque, J.-F., Emmons, L. K., Conley, A., Schultz, M. G., Saunois, M., Thouret, V., Thompson, A. M., Oltmans, S. J., Johnson, B., and Tarasick, D.: Technical Note: Ozonesonde climatology between 1995 and 2011: description, evaluation and applications, Atmos. Chem. Phys., 12, 7475–7497, https://doi.org/10.5194/acp-12-7475-2012, 2012.

Van Malderen, R., Allaart, M. A. F., De Backer, H., Smit, H. G. J., and De Muer, D.: On instrumental errors and related correction strategies of ozonesondes: possible effect on calculated ozone trends for the nearby sites Uccle and De Bilt, Atmos. Meas. Tech., 9, 3793–3816, https://doi.org/10.5194/amt-9-3793-2016, 2016.

Vicedo-Cabrera, A. M., Sera, F., Liu, C., Armstrong, B., Milojevic, A., Guo, Y., Tong, S., Lavigne, E., Kyselý, J., and Urban, A.: Short term association between ozone and mortality: global two stage time series study in 406 locations in 20 countries, British

Medical Journal, 368, m108, https://doi.org/10.1136/bmj.m108, 2020.

Wang, G., Kong, Q., Xuan, Y., Wan, X., Chen, H., and Ma, S.: Development and application of ozonesonde system in China, Adv. Earth Sci., 18, 471, https://doi.org/10.11867/j.issn.1001-8166.2003.03.0471, 2003.

Wang, H. J., Cunnold, D. M., Thomason, L. W., Zawodny, J. M., and Bodeker, G. E.: Assessment of SAGE version 6.1 ozone data quality, J. Geophys. Res.-Atmos., 107, ACH 8-1–ACH 8-18, 2002.

Wild, O., Voulgarakis, A., O'Connor, F., Lamarque, J.-F., Ryan, E. M., and Lee, L.: Global sensitivity analysis of chemistry–climate model budgets of tropospheric ozone and OH: exploring model diversity, Atmos. Chem. Phys., 20, 4047–4058, https://doi.org/10.5194/acp-20-4047-2020, 2020.

Witte, J. C., Thompson, A. M., Smit, H. G., Fujiwara, M., Posny, F., Coetzee, G. J., Northam, E. T., Johnson, B. J., Sterling, C. W., and Mohamad, M.: First reprocessing of Southern Hemisphere ADditional OZonesondes (SHADOZ) profile records (1998–2015): 1. Methodology and evaluation, J. Geophys. Res.-Atmos., 122, 6611–6636, 2017.

Witte, J. C., Thompson, A. M., Smit, H. G., Vömel, H., Posny, F., and Stübi, R.: First reprocessing of Southern Hemisphere ADditional OZonesondes profile records: 3. Uncertainty in ozone profile and total column, J. Geophys. Res.-Atmos., 123, 3243–3268, 2018.

Witte, J. C., Thompson, A. M., Schmidlin, F., Northam, E. T., Wolff, K. R., and Brothers, G. B.: The NASA Wallops Flight Facility digital ozonesonde record: Reprocessing, uncertainties, and dual launches, J. Geophys. Res.-Atmos., 124, 3565–3582, 2019.

WMO/GAW Ozone Monitoring Community, World Meteorological Organization-Global Atmosphere Watch Program (WMO-GAW): Ozone, World Ozone and Ultraviolet Radiation Data Centre (WOUDC) [data set], https://doi.org/10.14287/10000001, 2024.

Xu, W., Xu, X., Lin, M., Lin, W., Tarasick, D., Tang, J., Ma, J., and Zheng, X.: Long-term trends of surface ozone and its influencing factors at the Mt Waliguan GAW station, China – Part 2: The roles of anthropogenic emissions and climate variability, Atmos. Chem. Phys., 18, 773–798, https://doi.org/10.5194/acp-18-773-2018, 2018.

Xuan, Y., Ma, S., Chen, H., Wang, G., Kong, Q., Zhao, Q., and Wan, X.: Intercomparisons of GPSO3 and Vaisala ECC ozone sondes, Plateau Meteorology, 23, 394–399, 2004.

Young, P. J., Naik, V., Fiore, A. M., Gaudel, A., Guo, J., Lin, M. Y., Neu, J. L., Parrish, D. D., Rieder, H. E., Schnell, J. L., Tilmes, S., Wild, O., Zhang, L., Ziemke, J., Brandt, J., Delcloo, A., Doherty, R. M., Geels, C., Hegglin, M. I., Hu, L., Im, U., Kumar, R., Luhar, A., Murray, L., Plummer, D., Rodriguez, J., Saiz-Lopez, A., Schultz, M. G., Woodhouse, M. T., and Zeng, G.: Tropospheric Ozone Assessment Report: Assessment of global-scale model performance for global and regional ozone distributions, variability, and trends, Elementa: Science of the Anthropocene, 6, 10, https://doi.org/10.1525/elementa.265, 2018.

Zang, Z., Liu, J., Tarasick, D., Moeini, O., Bian, J., Thompson, A. M., Malderen, R. V., Smit, H. G. J., Stauffer, R. M., Johnson, B. J., and Kollonige, D. E. Trajectory-mapped Ozonesonde dataset for the Stratosphere and Troposphere, version 2 (TOST-v2) (Version Review), Zenodo [data set], https://doi.org/10.5281/zenodo.13984483, 2024.

Zbinden, R. M., Thouret, V., Ricaud, P., Carminati, F., Cammas, J.-P., and Nédélec, P.: Climatology of pure tropospheric profiles and column contents of ozone and carbon monoxide using MOZAIC in the mid-northern latitudes (24° N to 50° N) from 1994 to 2009, Atmos. Chem. Phys., 13, 12363–12388, https://doi.org/10.5194/acp-13-12363-2013, 2013.

Zeng, G., Morgenstern, O., Williams, J. H., O'Connor, F. M., Griffiths, P. T., Keeble, J., Deushi, M., Horowitz, L. W., Naik, V., and Emmons, L. K.: Attribution of stratospheric and tropospheric ozone changes between 1850 and 2014 in CMIP6 models, J. Geophys. Res.-Atmos., 127, e2022JD036452, https://doi.org/10.1029/2022JD036452, 2022.

Zeng, Y., Zhang, J., Li, D., Liao, Z., Bian, J., Bai, Z., Shi, H., Xuan, Y., Yao, Z., and Chen, H.: Vertical distribution of tropospheric ozone and its sources of precursors over Beijing: Results from∼ 20 years of ozonesonde measurements based on clustering analysis, Atmos. Res., 284, 106610, https://doi.org/10.1016/j.atmosres.2023.106610, 2023.

Zhang, J., Li, D., Bian, J., Xuan, Y., Chen, H., Bai, Z., Wan, X., Zheng, X., Xia, X., and Lü, D.: Long-term ozone variability in the vertical structure and integrated column over the North China Plain: Results based on ozonesonde and Dobson measurements during 2001–2019, Environ. Res. Lett., 16, 074053, https://doi.org/10.1088/1748-9326/ac109f, 2021.